Telefilters, telemirrors, and causality

Joshua Foo,[1,*] Sho Onoe,[1] Magdalena Zych,[2] and Timothy C. Ralph[1,†]
[1]*Centre for Quantum Computation and Communication Technology, School of Mathematics and Physics, University of Queensland, St. Lucia, Queensland 4072, Australia*
[2]*Centre for Engineered Quantum Systems, School of Mathematics and Physics, University of Queensland, St. Lucia, Queensland 4072, Australia*

(Received 25 June 2021; accepted 1 February 2022; published 18 March 2022)

We present theoretical models for quantum-optical mode-selective filters and mirrors using continuous-variable teleportation. We call these devices telefilters and telemirrors, respectively. Both devices act as the identity channel on a mode of interest from an input multimode field while filtering or reflecting all the orthogonal modes. We utilize these models to analyze a causality problem in relativistic quantum optics, specifically the apparently acausal transmission and propagation of temporally delocalized wave packets through mode-selective mirrors. First, we show how telemirrors, and thus mode-selective operations generally, enact a fundamental time delay on such wave packets, which is necessary in order to prevent violations of causality. We next consider teleporting the independent temporal components of the input field separately and continuously, that is, performing operations on the fly. In this scenario, the telemirror transmits the mode of interest as well as orthogonal modes which carry with them uncorrelated noise. In this scenario, the device may be considered mode discriminating but not mode selective.

DOI: 10.1103/PhysRevA.105.033711

I. INTRODUCTION

Unitary operations in quantum optics are defined by their action on single modes or between multiple modes of the electromagnetic field [1,2]. However, physical devices are usually only weakly selective of the modes which they act upon. For example, a beam splitter will typically allow a large number of different mode pairs to be mixed.

Mode-discriminating interactions [3] are more difficult to arrange physically but play an important role in quantum optics and interacting quantum field theories. Taking as input a multimode field, a mode-discriminating unitary affects a specific mode (for example, a spectral pulse) differently compared to modes orthogonal to it. A special class of mode-discriminating interactions is a mirror which transmits a single mode from a multimode input field and filters out or reflects all others. We refer to this specific kind of interaction where only one mode is transmitted as mode selective, to be distinguished from a mode-discriminating interaction which allows all modes to be transmitted while uniquely affecting one mode (conversely, affecting all but one mode). Mode-selective mirrors and beam splitters have been identified as key tools in future communications and metrology applications [4–8]. Other mode-discriminating interactions such as phase shifters, displacements, and squeezers have been studied in the context of relativistic quantum communication protocols [9–14] describing interactions between quantum fields and observers in relativistic reference frames.

Mode-selective operations have been realized experimentally. One notable example is the quantum pulse gate [15] which overlaps a weak input field with a strong classical gating pulse in a nonlinear crystal. Using a technique known as spectrally engineered sum-frequency generation, only the mode from the input field which matches the form of the gating pulse is converted into a wave packet at their sum frequency [16–19]. A frequency filter can then select the mode of interest. Another example is the Raman quantum memory [20], which interacts a train of control pulses with a signal mode inside an atomic vapor cell, yielding a controllable output which can be implemented as an optical beam-splitter network [21–23].

In this paper we propose a protocol for implementing the quantum-optical mode-selective mirror, using continuous-variable teleportation [24–26]. We first consider a general model which demonstrates a telefilter which transmits a specific single mode while blocking all others and then a telemirror which transmits a specific single mode while reflecting all others.

Next we develop a simplified model for a temporally delocalized wave packet, where an input state is distributed over two independent temporal modes [27–29] which interact with the mirror at earlier and later times (this is then extended to N temporal modes in Appendix D). Our motivation in studying this particular case is to understand how the interaction between temporally delocalized modes within mode-selective mirrors preserves causality, since such causal considerations are commonly neglected in theoretical models [17]. Indeed, as we show in Sec. IV, the standard unitary interaction between an input temporal mode and a mode-selective mirror leads to

*joshua.foo@uqconnect.edu.au
†ralph@physics.edu.au

superluminal signaling between the sender and receiver, due to the neglect of the above-mentioned causal considerations.

Using our models for the temporal-mode-selective filter and mirror (referring to them as temporal-mode telefilters and telemirror, respectively), we show that a fundamental time delay on the propagation of input modes is necessary in order for the action of such mirrors (and mode-selective mirrors generally) to remain consistent with relativity and to avoid violations of causality. Essentially, both the telefilter and telemirror enact what amounts to a measurement of the input wave packet (which we model as being constructed from discrete time-bin modes, with each mode measured in discrete succession), the duration of which is constrained by the temporal length of the wave packet itself. Obviously, performing such a measurement instantaneously is unphysical. Our results thus highlight some of the tacit assumptions within quantum-optical models for mode-selective interactions such as the Schmidt decomposition [3], which typically neglect time-ordering effects [17,30] and hence admit acausal solutions. In line with this, our approach may be considered a quantum-optical perspective on the important and ongoing discussion of causality-violating scenarios in relativistic quantum field theory, for example, in the context of Sorkin's impossible measurements [31–38].

Finally, we propose an alternative teleportation model for the mirror *without* a fundamental time delay, wherein the individual temporal components are teleported separately and continuously before being coherently recombined at an output port. We show that in general this model fails as a mode-selective mirror, instead allowing the selected mode *and* modes with the same temporal support but orthogonal to it to be transmitted. However, these orthogonal modes also carry additional sources of uncorrelated noise, thus only achieving a kind of mode discrimination as opposed to mode selectivity. The presence of the noise also limits the ability of a receiver to determine the arrival time of a signal (e.g., a photon) encoded in these modes; when this noise is very large, any attempt to determine arrival times will be thwarted. These properties of the no-delay telefilter and telemirror may have important consequences in applications such as quantum communication and quantum causality [39].

Our paper is organized as follows. In Sec. II we review the basic theoretical construction of mode-selective mirrors and the desired effect that they have upon an input multimode field. In Sec. III we review two approaches to continuous-variable teleportation. We then show how these teleportation protocols can function as mode-selective devices wherein a single mode of interest from an input field is transmitted to a receiver. In Sec. IV we highlight the neglect of causality considerations in standard models for mode-selective mirrors, which motivates us to generalize the telefilter and telemirror models to an input of two independent temporal modes. We introduce and study this model in Sec. V, showing that it enacts an unavoidable time delay upon the mode of interest as it propagates between the sender and receiver. In Sec. VI we introduce the alternative model for the temporal-mode telemirror and telefilter where the temporal components are teleported separately and continuously. We offer some conclusions and implications of our results in Sec. VII.

Throughout this paper, we utilize natural units $\hbar = c = 1$.

II. MODE-SELECTIVE MIRRORS

Before introducing our model for the mode-selective mirror, we review a standard theoretical implementation of such a mirror and the transformation it enacts upon incoming field modes.

First, consider a complete set of orthonormal modes $\{\hat{a}_l\}$ within which the mode of interest $\hat{a}_0$ is contained. Likewise, we introduce a matching set of orthonormal modes $\{\hat{b}_l\}$ which are orthogonal to $\{\hat{a}_l\}$ and contain the mode $\hat{b}_0$, which is complementary to $\hat{a}_0$. By matching, we mean that $\{\hat{a}_l\}$ and $\{\hat{b}_l\}$ are in the same mode, allowing them to interact at a beam splitter. We wish to construct a mode-selective unitary which only affects the mode of interest $\hat{a}_0$ and its complement incident from the other direction $\hat{b}_0$.

To highlight the effect of a mode-selective unitary on the incident modes $\{\hat{a}_l\}$ and $\{\hat{b}_l\}$, it is instructive to contrast this with that of a passive or non-mode-selective unitary. A non-mode-selective beam-splitter interaction can be modeled via the unitary

$$\hat{U} = \exp\left[-i\theta\left(\sum_l \hat{a}_l \hat{b}_l^\dagger + \text{H.c.}\right)\right]. \tag{1}$$

Consider an incoming mode $\hat{a}_{\text{in}}$, constructed as a superposition of the modes in $\{\hat{a}_l\}$,

$$\hat{a}_{\text{in}} = \sum_l f_l \hat{a}_l, \tag{2}$$

where $\sum_l |f_l|^2 = 1$, interacting with the other set of incident modes $\{\hat{b}_l\}$. If we prepare the single-photon state $\hat{a}_{\text{in}}^\dagger|0\rangle$ (where $|0\rangle$ is the state annihilated by the operators $\{\hat{a}_l\}$ and $\{\hat{b}_l\}$ and the $\hat{b}_l$ modes are in the vacuum) and apply Eq. (1) to it, we find, using the Baker-Campbell-Hausdorff formula, that

$$\hat{U}\hat{a}_{\text{in}}^\dagger|0\rangle = \left(\cos\theta \sum_l f_l^\star \hat{a}_l^\dagger - i\sin\theta \sum_l f_l^\star \hat{b}_l^\dagger\right)|0\rangle. \tag{3}$$

This is the well-known input-output relationship for the interaction of $\hat{a}_{\text{in}}$ and $\hat{b}_{\text{in}}$ at a passive beam splitter and is true for any choice of f_l. Note especially that Eq. (1) affects all of the constituent modes in $\hat{a}_{\text{in}}$ and $\hat{b}_{\text{in}}$ unilaterally and cannot be considered mode selective.

To understand the action of a mode-selective mirror on the input modes, let us decompose $\hat{a}_{\text{in}}$ as [3]

$$\hat{a}_{\text{in}} = [\hat{a}_{\text{in}}, \hat{a}_0^\dagger]\hat{a}_0 + \sum_{l\neq 0} f_l \hat{a}_l, \tag{4}$$

where $|[\hat{a}_{\text{in}}, \hat{a}_0^\dagger]|^2 + \sum_{l\neq 0} |f_l|^2 = 1$ enforces normalization. This technique is known as the Schmidt decomposition [40] and is widely used in quantum information and optics as a way of decomposing generic states into arbitrary bases of orthogonal modes [41–43].

A common approach is to use the unitary [17]

$$\hat{U}_0 = \exp[-i\theta(\hat{a}_0\hat{b}_0^\dagger + \text{H.c.})], \tag{5}$$

where $0 \leqslant \theta \leqslant \pi/2$. Equation (5) takes a form similar to the passive beam-splitter unitary of Eq. (1); however, the key difference is that from the complete sets $\{\hat{a}_l\}$ and $\{\hat{b}_l\}$, it only affects $\hat{a}_0$ and $\hat{b}_0$. To see this, let us again prepare a

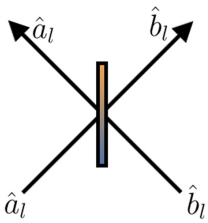

FIG. 1. Geometry of the mode propagation through the mirror, where the $\{\hat{b}_l\}$ modes refer to the transmitted modes, compared with the $\{\hat{a}_l\}$ modes, referring to those reflected. Our slightly nonstandard labeling of the transmitted and reflected modes is done to retain consistency with later parts of the paper, in which the right-moving mode is always the transmitted one.

single-photon state $\hat{a}_{\rm in}^\dagger|0\rangle$ and apply the unitary of Eq. (5) to it, yielding

$$\hat{U}_0\hat{a}_{\rm in}^\dagger|0\rangle = \left([\hat{a}_{\rm in},\hat{a}_0^\dagger]^\star(\hat{a}_0^\dagger\cos\theta - i\hat{b}_0^\dagger\sin\theta) + \sum_{l\neq 0} f_l^\star\hat{a}_l^\dagger\right)|0\rangle, \tag{6}$$

where we have utilized the properties $\hat{U}_0\hat{U}_0^\dagger = \mathbb{I}$ and $\hat{U}_0|0\rangle = |0\rangle$. If we consider $\theta = \pi/2$, we obtain

$$\hat{U}_0\hat{a}_{\rm in}^\dagger|0\rangle = \left(-i[\hat{a}_{\rm in},\hat{a}_0^\dagger]^\star\hat{b}_0^\dagger + \sum_{l\neq 0} f_l^\star\hat{a}_l^\dagger\right)|0\rangle. \tag{7}$$

Note that our choice of $\theta = \pi/2$ corresponds to the selected mode being transmitted through the mirror; the geometry of the mode propagation is shown in Fig. 1. The overlap of $\hat{a}_0$ and $\hat{a}_{\rm in}$ has been transmitted into the $\hat{b}_0$ mode, while the orthogonal modes $\hat{a}_{l\neq 0}$ are reflected by the mirror. Likewise, when considering the effect of Eq. (5) upon the $\hat{b}_0$ mode incident from the other side of the mirror, we find that it too is completely transmitted into the $\hat{a}_0$ mode: $\hat{U}_0^\dagger\hat{b}_0\hat{U}_0 = i\hat{a}_0$. Thus, Eq. (6) transmits a single mode (the 0 mode) from the multimode input, while the orthogonal modes $\hat{a}_l$ are reflected to the other side. The desired outcome is achieved, namely, the isolation of a single mode from the input field.

III. CONTINUOUS-VARIABLE TELEPORTATION AS MODE SELECTIVITY

In this section we introduce the homodyne measurement and all-optical approaches to continuous-variable (CV) teleportation of an input mode. These simple models highlight the mode-selective property of such teleporters, wherein a single mode from the input is transmitted through the circuit while all orthogonal modes are filtered or reflected. This achieves an analogous input-output transformation to the unitary of Eq. (5).

A. Homodyne measurement telefilter

Quantum teleportation is the process whereby an unknown input state $\hat{\rho}_{\rm in}$ is transferred between distant observers using a classical channel and a preexisting entanglement resource. The seminal work by Bennett *et al.* [24] utilized entangled Bell pairs as the resource; however, this was later extended

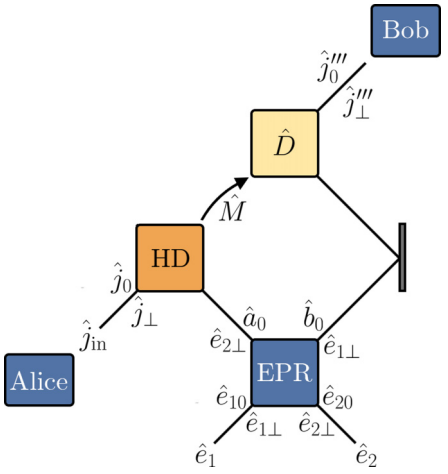

FIG. 2. Schematic diagram of CV teleportation using a homodyne measurement of the input mode $\hat{j}_{\rm in}$ with the entanglement resource mode $\hat{a}_0$. The shaded mirror on the right is non-mode-selective, perfectly reflecting and simply included for aesthetic purposes; the left-moving complement mode incident on the other side is irrelevant to the protocol. The details of the homodyne measurement are illustrated in Fig. 4.

to CV protocols by Vaidman [25] and Braunstein and Kimble [26]. Essentially, a bipartite entangled system is shared between a sender and receiver, who perform local operations and communicate via classical channels so that the receiver can retrieve an arbitrarily good version of the initial state $\hat{\rho}_{\rm in}$, without the direct transmission of quantum information between them. A comprehensive review of CV teleportation can be found in the article by Pirandola and Mancini [44].

Throughout this paper, we will describe our quantum-optical protocols in the Heisenberg picture [1]. The first approach is illustrated in the circuit diagram in Fig. 2, which utilizes a distributed entanglement resource and a dual homodyne measurement to achieve mode-selective CV teleportation. First, Alice receives an input mode $\hat{j}_{\rm in}$ in an arbitrary state. As discussed previously, $\hat{j}_{\rm in}$ can be decomposed in the basis of constituent orthonormal modes $\{\hat{j}_0, \hat{j}_\perp\}$ which copropagate in the same beam. This decomposition is illustrated schematically in Fig. 3. She aims to select, that is, transmit, $\hat{j}_0$ (more precisely, the overlap of $\hat{j}_{\rm in}$ with $\hat{j}_0$) to Bob, while filtering out $\hat{j}_\perp$.

To achieve this, Alice enacts the dual homodyne measurement (outlined in detail below) of $\hat{j}_0$ mixed with her half of the

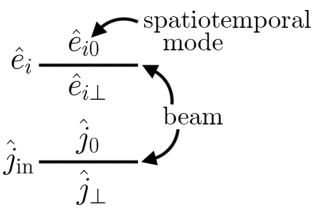

FIG. 3. Schematic representation of the mode decomposition of the spatiotemporal modes $\hat{e}_i$ and $\hat{j}_{\rm in}$. The orthogonal modes $\{\hat{e}_{i0}, \hat{e}_{i\perp}\}$ and $\{\hat{j}_0, \hat{j}_\perp\}$ respectively copropagate in the same beam, denoted by the solid black line.

entanglement resource mode $\hat{a}_0$. The entanglement resource modes are generated by two-mode squeezing of the vacuum modes $\hat{e}_i$. Just like Alice's input mode, the input vacua can be decomposed in the orthonormal basis $\{\hat{e}_{i0}, \hat{e}_{i\perp}\}$; these modes likewise copropagate in the same beam. The $\hat{e}_{i0}$ modes are spatiotemporally mode matched with the mode of interest $\hat{j}_0$. The two-mode squeezer unitary

$$\hat{S}_2(s) = \exp(\xi^\star \hat{e}_{10}\hat{e}_{20} - \xi \hat{e}_{10}^\dagger \hat{e}_{20}^\dagger) \tag{8}$$

generates the transformation on the $\hat{e}_{i0}$ modes,

$$\hat{a}_0 = \hat{S}_2^\dagger(s)\hat{e}_{10}\hat{S}_2(s) = \cosh(s)\hat{e}_{10} + \sinh(s)\hat{e}_{20}^\dagger, \tag{9}$$

$$\hat{b}_0 = \hat{S}_2^\dagger(s)\hat{e}_{20}\hat{S}_2(s) = \cosh(s)\hat{e}_{20} + \sinh(s)\hat{e}_{10}^\dagger, \tag{10}$$

where $\xi = se^{i\varphi}$, $\cosh(s)$ is the squeezing gain, and φ controls the relative phase between the vacuum modes in Eqs. (9) and (10). In the Schrödinger picture, acting the two-mode squeezer on the vacuum creates the well-known Einstein-Podolsky-Rosen (EPR) state (or two-mode squeezed state) $|s\rangle_{\rm EPR} = \hat{S}_2(s)|0\rangle$ (hence our choice of label in Fig. 2 and throughout this paper). In the limit $s \to \infty$, $\hat{a}_0$ and $\hat{b}_0$ become perfectly entangled. The two-mode squeezing interaction could be mediated by a $\chi^{(2)}$ nonlinear crystal in which the shape of the pump field is mode matched to the $\hat{e}_{i0}$ modes. We note here that the squeezer is mode discriminating (not mode selective); while it selectively generates a two-mode squeezed state of the $\hat{e}_{i0}$ vacuum modes, the $\perp$ modes are still transmitted through the optical element without being affected. One recalls that our definition of mode discrimination is to be distinguished from mode selectivity, the latter being the desired property of the mirror where only the mode of interest is transmitted, while the orthogonal modes are filtered or reflected. The entanglement resource modes $\hat{a}_0$ and $\hat{b}_0$ are distributed to the two participants Alice and Bob.

Let us return to Alice and her input mode $\hat{j}_{\rm in}$, which can be expressed as a superposition of the constituent orthonormal basis modes

$$\hat{j}_{\rm in} = f_0\hat{j}_0 + \sum_{l\neq 0} f_l \hat{j}_l \tag{11}$$

alongside its orthogonal complement $\hat{j}_{{\rm in},\perp}$,

$$\hat{j}_{{\rm in},\perp} = \sqrt{1-|f_0|^2}\,\hat{j}_0 - \frac{f_0}{\sqrt{1-|f_0|^2}}\sum_{l\neq 0} f_l \hat{j}_l, \tag{12}$$

where $\sum_l |f_l|^2 = 1$. By making the association $\sqrt{\epsilon} = f_0$, Eqs. (11) and (12) can be recast into beam-splitter-type relations

$$\hat{j}_{\rm in} = \sqrt{\epsilon}\,\hat{j}_0 + \sqrt{1-\epsilon}\,\hat{j}_\perp, \tag{13}$$

$$\hat{j}_{{\rm in},\perp} = \sqrt{1-\epsilon}\,\hat{j}_0 - \sqrt{\epsilon}\,\hat{j}_\perp, \tag{14}$$

where we have defined

$$\hat{j}_\perp = \frac{1}{\sqrt{1-|f_0|^2}}\sum_{l\neq 0} f_l \hat{j}_l. \tag{15}$$

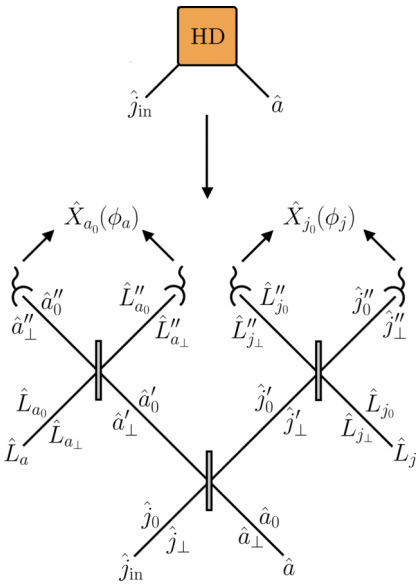

FIG. 4. Circuit diagram of the homodyne detection scheme. Here $\hat{j}_{\rm in}$ and $\hat{a}$ are mixed on a balanced beam splitter. The measurement results are used to construct the operator $\hat{M}$. Referring to our dual-rail representation of the modes (see Fig. 3), each line here represents a beam within which the orthogonal modes denoted by 0 and $\perp$ copropagate.

Inverting Eqs. (13) and (14), we obtain the following form for the constituent modes:

$$\hat{j}_0 = \sqrt{\epsilon}\,\hat{j}_{\rm in} + \sqrt{1-\epsilon}\,\hat{j}_{{\rm in},\perp}, \tag{16}$$

$$\hat{j}_\perp = \sqrt{1-\epsilon}\,\hat{j}_{\rm in} - \sqrt{\epsilon}\,\hat{j}_{{\rm in},\perp}. \tag{17}$$

The dual homodyne measurement performed by Alice is a widely used technique in quantum optics [1]. This process, which is a CV equivalent of a Bell measurement, is illustrated in Fig. 4. First, Alice mixes $\hat{j}_{\rm in}$ and $\hat{a}$ (i.e., their constituent modes) at a balanced, passive beam splitter, yielding

$$\hat{j}_0' = \frac{1}{\sqrt{2}}(\hat{a}_0 + \hat{j}_0), \quad \hat{a}_0' = \frac{1}{\sqrt{2}}(\hat{j}_0 - \hat{a}_0),$$
$$\hat{j}_\perp' = \frac{1}{\sqrt{2}}(\hat{a}_\perp + \hat{j}_\perp), \quad \hat{a}_\perp' = \frac{1}{\sqrt{2}}(\hat{j}_\perp - \hat{a}_\perp). \tag{18}$$

Alice prepares two local oscillator modes $\hat{L}_j$ and $\hat{L}_a$, which can be similarly represented in a complete basis of orthogonal modes $\{\hat{L}_{j_0}, \hat{L}_{j_\perp}\}$ and $\{\hat{L}_{a_0}, \hat{L}_{a_\perp}\}$, respectively. The subscripts denote the modes which the local oscillators are matched to. The local oscillators matching the 0 modes are assumed to be prepared in large-amplitude coherent states, written in the form

$$\hat{L}_i = \beta + \delta\hat{L}_i, \quad \text{where} \quad i = j_0, a_0, \tag{19}$$

with $\beta = |\beta|e^{-i\phi_i} = \langle \hat{L}_i\rangle \gg 1$ and $\delta\hat{L}_i = \hat{L}_i - \beta$, while the orthogonal local oscillator modes are vacuum modes given by [1]

$$\hat{L}_k = \delta\hat{L}_k, \quad \text{where} \quad k = j_\perp, a_\perp. \tag{20}$$

We have utilized the nomenclature $\delta\hat{L}_k$ to emphasize that these modes have zero mean. Alice interacts the input modes (18) with the respective local oscillator modes at balanced, passive beam splitters, yielding

$$\hat{j}_0'' = \frac{1}{\sqrt{2}}(\hat{j}_0' + \hat{L}_{j_0}), \quad \hat{L}_{j_0}'' = \frac{1}{\sqrt{2}}(\hat{L}_{j_0} - \hat{j}_0'),$$
$$\hat{a}_0'' = \frac{1}{\sqrt{2}}(\hat{a}_0' + \hat{L}_{a_0}), \quad \hat{L}_{a_0}'' = \frac{1}{\sqrt{2}}(\hat{L}_{a_0} - \hat{a}_0') \tag{21}$$

and likewise

$$\hat{j}_\perp'' = \frac{1}{\sqrt{2}}(\hat{j}_\perp' + \hat{L}_{j_\perp}), \quad \hat{L}_{j_\perp}'' = \frac{1}{\sqrt{2}}(\hat{L}_{j_\perp} - \hat{j}_\perp'),$$
$$\hat{a}_\perp'' = \frac{1}{\sqrt{2}}(\hat{a}_\perp' + \hat{L}_{a_\perp}), \quad \hat{L}_{a_\perp}'' = \frac{1}{\sqrt{2}}(\hat{L}_{a_\perp} - \hat{a}_\perp'). \tag{22}$$

Using the modes in Eqs. (21) and (22), we first construct number operators at the respective detectors

$$\hat{N}_k = \hat{k}^\dagger\hat{k}, \quad \text{where} \quad k = a_0'', a_\perp'', j_0'', j_\perp'',$$
$$\hat{N}_l = \hat{l}^\dagger\hat{l}, \quad \text{where} \quad l = L_{a_0}'', L_{a_\perp}'', L_{j_0}'', L_{j_\perp}'', \tag{23}$$

which are then added together as

$$\hat{N}_a = \hat{N}_{a_0''} + \hat{N}_{a_\perp''}, \quad \hat{N}_{L_a} = \hat{N}_{L_{a_0}''} + \hat{N}_{L_{a_\perp}''},$$
$$\hat{N}_j = \hat{N}_{j_0''} + \hat{N}_{j_\perp''}, \quad \hat{N}_{L_j} = \hat{N}_{L_{j_0}''} + \hat{N}_{L_{j_\perp}''}. \tag{24}$$

The photon numbers at the respective ports are subtracted to obtain the output signal operators $\hat{O}_j = \hat{N}_j - \hat{N}_{L_j}$ and $\hat{O}_a = \hat{N}_a - \hat{N}_{L_a}$, yielding

$$\hat{O}_j = \hat{j}_0'^\dagger\hat{L}_{j_0} + \hat{L}_{j_0}^\dagger\hat{j}_0' + \hat{j}_\perp'^\dagger\hat{L}_{j_\perp} + \hat{L}_{j_\perp}^\dagger\hat{j}_\perp', \tag{25}$$

$$\hat{O}_a = \hat{a}_0'^\dagger\hat{L}_{a_0} + \hat{L}_{a_0}^\dagger\hat{a}_0' + \hat{a}_\perp'^\dagger\hat{L}_{a_\perp} + \hat{L}_{a_\perp}^\dagger\hat{a}_\perp'. \tag{26}$$

By applying the definition of Eq. (19) and neglecting terms not multiplied by the coherent signal β, we find that

$$\hat{O}_j = |\beta|\hat{X}_{j_0'}(\phi_j) = |\beta|(e^{-i\phi_j}\hat{j}_0' + e^{i\phi_j}\hat{j}_0'^\dagger), \tag{27}$$

$$\hat{O}_a = |\beta|\hat{X}_{a_0'}(\phi_a) = |\beta|(e^{-i\phi_a}\hat{a}_0' + e^{i\phi_a}\hat{a}_0'^\dagger). \tag{28}$$

In quantum optics, the quadrature operators $\hat{X}_{j_0}(\phi_j)$ and $\hat{X}_{a_0}(\phi_a)$ (of the modes denoted in the subscript) can be used to reconstruct the Wigner function of a state through measurements of their amplitudes via homodyne detection [1]. They are characterized by their amplitude β and phase ϕ_i in phase space and in this context represent the classical statistics of the measurement. By taking ϕ_a and ϕ_j to be $\pi/2$ out of phase, Alice can subsequently construct an operator $\hat{M}$ from this joint measurement, for example,

$$\hat{M} = |\beta|\left(\hat{X}_{j_0'} + i\hat{P}_{a_0'}\right) = \sqrt{2}|\beta|(\hat{j}_0 + \hat{a}_0^\dagger), \tag{29}$$

which satisfies $[\hat{M}, \hat{M}^\dagger] = 0$ and we have adopted the nomenclature

$$\hat{X}_i = \hat{X}_i(\phi_i = 0), \quad \hat{P}_i = \hat{X}_i(\phi_i = \pi/2). \tag{30}$$

Here $\hat{M}$ represents the classical channel which Alice sends to Bob [45], who subsequently uses it to displace[1] his half of the entangled pair [1],

$$\hat{j}_0''' = \hat{b}_0 + \zeta\hat{M}, \tag{31}$$

where $\zeta \in \mathbb{C}$ is the effective gain of the classical channel. Taking $\zeta = 1/\sqrt{2}|\beta|$ yields a unity gain channel between Alice and Bob so that Bob's mode becomes

$$\hat{j}_0''' = -\hat{j}_0 + (\hat{b}_0 - \hat{a}_0^\dagger). \tag{32}$$

Using Eqs. (9) and (10), we find that in the limit of perfect entanglement ($s \to \infty$),

$$\lim_{s\to\infty}\hat{j}_0''' = -\hat{j}_0, \quad \hat{j}_\perp''' = \hat{e}_{1\perp}, \tag{33}$$

that is, Bob perfectly retrieves the overlap of Alice's mode with the mode of interest $\hat{j}_0$ (modulo an arbitrary global phase). Notice that the orthogonal mode $\hat{j}_\perp$ is filtered out at the measurement while the copropagating mode $\hat{e}_{1\perp}$ is in the vacuum.

To reiterate why the teleporter is mode selective, recall that only the mode of interest $\hat{j}_0$ is matched to and consequently amplified by the large-amplitude local oscillator mode. Likewise, the entanglement resource $\hat{a}_0$ is prepared in the same spatiotemporal mode as $\hat{j}_0$ and $\hat{L}_{a_0}$. The sets of orthogonal modes $\{\hat{j}_\perp\}$ and $\{\hat{a}_\perp\}$ are filtered out at the level of the detection process, since they are not mixed with the large-amplitude local oscillator modes and can be neglected as small. Thus, their unamplified quadratures are hidden beneath the semiclassical noise of the large-amplitude coherent state. In view of this, we refer to the circuit of Fig. 2 as a mode-selective telefilter. This is an analogous scenario to Eq. (6), where the mode of interest was transmitted while all others were reflected. For our purposes, they achieve an identical outcome in terms of the isolation of the desired mode. We finally note that the mode-selective properties of homodyne detection are well known [5,46–48]; however here we utilize this property to achieve the mode-selective transmission of a particular mode from an input field, in the context of CV teleportation.

B. Telefilters with imperfect efficiency

The previous model for the single-mode telefilter was characterized by a unity gain channel between Alice and Bob; $\hat{j}_0$ is teleported between them without loss, and the efficiency of the protocol is effectively characterized by the additional noise carried by the entanglement resource modes. In the limit of infinite squeezing, the noise from these modes vanishes.

It is instructive to consider a nonunity gain channel between Alice and Bob, when the squeezing is finite. Such a scenario represents a telefilter with imperfect efficiency; for

[1]In the Heisenberg picture, the action of the unitary displacement operator $\hat{D}(\alpha) = \exp(\alpha\hat{a}^\dagger - \alpha^\star\hat{a})$ for the arbitrary complex number $\alpha = |\alpha|e^{i\theta}$ is given by $\hat{D}^\dagger(\alpha)\hat{a}\hat{D}(\alpha) = \hat{a} + \alpha$ and $\hat{D}^\dagger(\alpha)\hat{a}^\dagger\hat{D}(\alpha) = \hat{a}^\dagger + \alpha^\star$ [1]. In the present case, $\hat{M}$ can be interpreted as a complex number.

finite squeezing, some of the input mode is actually lost. Recall that Bob's output displaced mode is given by Eq. (31),

$$\hat{j}_0''' = \hat{b}_0 + \zeta \hat{M}. \tag{34}$$

By taking the effective gain to be the squeezing-dependent function $\zeta = \tanh(s)/\sqrt{2}|\beta|$ [49], we find that the output mode reduces to

$$\hat{j}_0''' = \tanh(s)\hat{j}_0 + \frac{\hat{e}_{20}}{\cosh(s)}. \tag{35}$$

Since $\tanh(s)$ is a monotonically increasing function of the squeezing parameter s within the range [0,1], this determines how much of the input mode is successfully teleported (i.e., transmitted through the filter). In the limit of infinite squeezing, the coefficient of $\hat{e}_{20}$ vanishes, leaving $\hat{j}_0$ exactly. In this sense, the telefilter may be understood as a filter with a variable transmission coefficient determined by the squeezing parameter s. As we discuss in Appendix B, this calculation generalizes to an N-mode input.

C. All-optical telemirror

An alternative approach to CV teleportation is the all-optical protocol first proposed by Ralph in [50]. The difference between the all-optical and homodyne measurement protocols is that the former does not directly enact a "measurement" on the input mode and is thus entirely unitary. Apart from this difference, the two approaches are functionally equivalent in terms of the teleported beam. Notably, the all-optical protocol has been recently realized in experiment [51] and has also been recently studied in the context of relativistic noninertial observers [12]. The circuit diagram for the protocol is shown in Fig. 5. It can be straightforwardly shown that this is an equivalent approach to the previous case studied, using homodyne measurements. Unlike the telefilter, the input mode of interest $\hat{j}_0$ is mixed with the entangled mode $\hat{a}_0$ at a two-mode squeezer. The two-mode squeezer creates the classical channel between Alice and Bob by highly amplifying the input mode $\hat{j}_0$ along with $\hat{a}_0$, producing the mode $\hat{c}_0$. The quadratures of $\hat{c}_0$ have uncertainty significantly larger than the quantum noise limit of unity. Any noise introduced by a joint measurement of $\hat{X}_{c_0}$ and $\hat{P}_{c_0}$ is negligible compared to these already amplified amplitudes, warranting the designation of $\hat{c}_0$ as a classical field [50].

This is where the mode selectivity of the all-optical teleporter becomes manifest. As already mentioned, the two-mode squeezing interaction can be controlled by the shape of the pump field inside a $\chi^{(2)}$ nonlinear crystal, mode matched with the mode to be squeezed. Here we assume that $\hat{j}_0$ and $\hat{a}_0$ are mode matched with the mode-discriminating squeezer, while the orthogonal modes $\hat{j}_\perp$ and $\hat{a}_\perp$ pass through the crystal unaffected.

Now the transformation which $\hat{S}_2(r)$ enacts upon the modes is expressed as

$$\hat{c}_0 = \cosh(r)\hat{j}_0 + \sinh(r)\hat{a}_0^\dagger, \tag{36}$$

$$\hat{a}_0' = \cosh(r)\hat{a}_0 + \sinh(r)\hat{j}_0^\dagger. \tag{37}$$

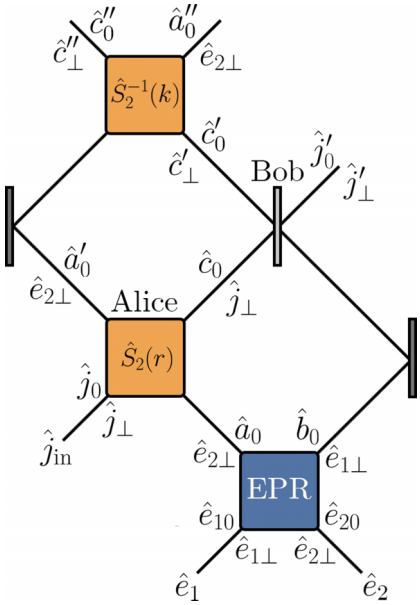

FIG. 5. Schematic diagram of the all-optical teleportation circuit. The homodyne measurement is replaced by a two-mode squeezer, denoted by $\hat{S}_2(r)$. Note especially that the $\perp$ modes are unaffected by the squeezing elements; hence they retain their labels as they propagate through these elements, whereas the 0 modes are transformed by the squeezers. Both the $\perp$ and 0 modes are affected by the non-mode-selective beam splitters (the leftmost and rightmost mirrors).

In the limit of high gain ($r \gg 1$) the operator $\hat{c}_0$ is identical to the measurement operator in Eq. (29) (modulo an arbitrarily chosen squeezing phase between $\hat{j}_0$ and $\hat{a}_0$; we have chosen a plus sign between them as the convention for the main text of this paper) for a large coherent amplitude $|\beta| \gg 1$. This emphasizes the direct mapping between the two approaches at each stage of the protocol. As mentioned, the orthogonal modes pass through the squeezer unaffected. Bob uses a passive beam splitter to mix his part of the entanglement $\hat{b}_0$ with the classical channel. The output takes the form

$$\hat{j}_0' = \sqrt{\eta}\hat{c}_0 - \sqrt{1-\eta}\hat{b}_0, \tag{38}$$

$$\hat{j}_\perp' = \sqrt{\eta}\hat{j}_\perp - \sqrt{1-\eta}\hat{e}_{1\perp}. \tag{39}$$

Meanwhile, the reflected $\hat{c}$ modes are given by

$$\hat{c}_0' = \sqrt{\eta}\hat{b}_0 + \sqrt{1-\eta}\hat{c}_0, \tag{40}$$

$$\hat{c}_\perp' = \sqrt{\eta}\hat{e}_{1\perp} + \sqrt{1-\eta}\hat{j}_\perp. \tag{41}$$

Again, notice that Eq. (38) is analogous to Eq. (31) up to some phase determined by the squeezing angle and the beam-splitter phase. By setting $\eta = \cosh^{-2}(r)$ (i.e., most of the channel is reflected), this becomes

$$\hat{j}_0' = \hat{j}_0 - \tanh(r)(\hat{b}_0 - \hat{a}_0^\dagger), \tag{42}$$

$$\hat{j}_\perp' = \frac{1}{\cosh(r)}\hat{j}_\perp - \tanh(r)\hat{e}_{1\perp}. \tag{43}$$

In the limit of high entanglement between the resource modes ($r \to \infty$), the outputs reduce to

$$\hat{j}'_0 = \hat{j}_0, \quad \hat{j}'_\perp = -\hat{e}_{1\perp}, \tag{44}$$

that is, Bob reconstructs the overlap of Alice's mode with the mode of interest $\hat{j}_0$ with the vacuum mode $\hat{e}_{1\perp}$ copropagating with it. We thus see that both the homodyne measurement and all-optical approaches yield the same desired outcome, namely, the transmission of a selected mode of interest. Importantly, the mode selection achieved by the protocol maps the input to the output in the same spatiotemporal mode. In comparison with the mode-selective telefilter, this protocol is entirely unitary, which makes it possible to retrieve the reflected mode on Alice's side as well. For this reason, we refer to the all-optical teleporter as a mode-selective telemirror.

To determine the form of the reflected modes, one can perform an inverse squeezing operation, denoted by $\hat{S}_2^{-1}(k)$, which retrieves (in the limit of infinite squeezing on both the entanglement and classical channel) the input vacua,

$$\lim_{r,s\to\infty} \hat{c}''_0 = \hat{e}_{10}, \quad \lim_{r,s\to\infty} \hat{a}''_0 = \hat{e}_{20}. \tag{45}$$

Likewise in the reflected $\perp$ modes, one retrieves the mode orthogonal to $\hat{j}_0$ ($\hat{j}_\perp$) in the limit of infinite squeezing

$$\lim_{r,s\to\infty} \hat{c}''_\perp = \hat{j}_\perp \tag{46}$$

(since the beam-splitter transmission controlled by Bob is dependent on the squeezing r), as well as the remaining vacuum mode ($\hat{e}_{2\perp}$). This confirms that the teleportation protocol is fully unitary. The $\hat{j}_\perp$ mode orthogonal to $\hat{j}_0$ is reflected by the telemirror, since it does not interact with $\hat{S}_2(r)$. Finally, we note that as with the telefilter protocol, a similar calculation can be performed to obtain a telemirror with imperfect efficiency, which we present in Appendix B.

IV. CAUSALITY CONSIDERATIONS IN MODE-SELECTIVE INTERACTIONS

In the previous sections we reviewed two well-known CV teleportation protocols. By decomposing the input mode into copropagating orthogonal components, we showed that such protocols act as mode-selective devices, transmitting the mode of interest $\hat{j}_0$ and filtering or reflecting its orthogonal complement mode $\hat{j}_\perp$. However, in these protocols, and more generally mode-selective interactions of the form of Eq. (5), the temporal properties of the input mode are neglected, as are any causal considerations affecting the propagation of such modes between Alice and Bob. The implicit assumption of these previous protocols is that the time taken to enact the homodyne measurement is short. Any delay induced by the measurement time of the mode is effectively negligible in protocols such as Fig. 2.

This scenario is illustrated schematically in Fig. 6(a), where the mirror is likewise short in time. For this reason, we henceforth refer to the teleportation protocols discussed in Sec. III as atemporal representations of the telefilter and telemirror. Our aim for the remainder of this paper is to generalize our mode-selective teleportation model so that it captures, in the simplest way, the causality effects involved in

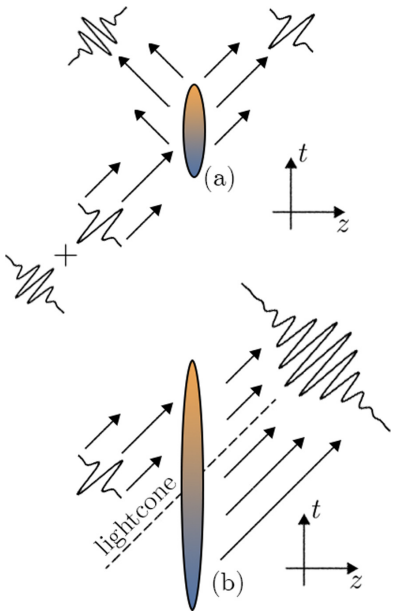

FIG. 6. Schematic representation of the causality issues arising from the action of mode-selective mirrors. (a) Scenario similar to the mode-selective telemirror, where we have neglected the temporal aspects of the problem. (b) The action of the mirror occurs over some delocalized time window, which allows for superluminal signaling (communication outside the lightcone) if instantaneous measurements are permitted. In particular, the transmitted mode has nonzero probability of the photon appearing in regions that are spacelike separated from the region in which the input pulse is located.

the propagation of temporal modes [27–29,52] through such mode-selective devices. This will be achieved by introducing a discrete non-negligible temporal extent to the input mode and likewise to the mirror unitary itself.

The standard mode-selective unitary of Eq. (5) is not adequate for such a treatment, because it admits causality-violating scenarios. Consider Fig. 6(b), in which the input mode only partially overlaps with the temporally extended mode-selective mirror. Since the temporal extent of the mode which the mirror selects is longer than that of the input mode, one can arrive at causality-violating scenarios in which superluminal signaling is possible if the mode-selective mirror acts instantaneously. To see this explicitly, consider the toy model modification of the unitary beam-splitter interaction of Eq. (5),

$$\hat{U}_0 = \exp\left(-\frac{i\theta}{2}[(\hat{a}_E + \hat{a}_L)(\hat{b}_E^\dagger + \hat{b}_L^\dagger) + \text{H.c.}]\right), \tag{47}$$

where $\{\hat{a}_E, \hat{a}_L\}$ and $\{\hat{b}_E, \hat{b}_L\}$ are temporal modes (the subscripts denoting early and late modes, respectively). The mirror now acts over the extended time window spanned by the early and late modes and selects and only transmits the symmetric superposition of $\hat{a}_E$ and $\hat{a}_L$. Now suppose that we inject a photon into the late mode $\hat{a}_{\text{in}} = \hat{a}_L$. It can be shown

that the output state after the interaction is given by

$$\hat{U}_0\hat{a}_L^\dagger|0\rangle = \left(\frac{1}{2}(\cos\theta+1)\hat{a}_E^\dagger + \frac{1}{2}(\cos\theta-1)\hat{a}_L^\dagger - \frac{i}{2}\sin\theta(\hat{b}_E^\dagger+\hat{b}_L^\dagger)\right)|0\rangle. \tag{48}$$

Setting $\theta = \pi/2$ (perfect transmission) yields

$$\hat{U}_0\hat{a}_L^\dagger|0\rangle = \left(\frac{1}{2}(\hat{a}_E^\dagger-\hat{a}_L^\dagger) - \frac{i}{2}(\hat{b}_E^\dagger+\hat{b}_L^\dagger)\right)|0\rangle. \tag{49}$$

We see that the symmetric superposition $(\hat{b}_E+\hat{b}_L)/\sqrt{2}$ has been transmitted by the mirror, while the antisymmetric superposition $(\hat{a}_E-\hat{a}_L)/\sqrt{2}$ has been reflected (following the prescriptions for the transmitted and reflected mode labels introduced in Fig. 1). The violation of causality produced by the unitary of Eq. (47) can be seen by projecting onto the early and late modes, respectively. Projecting onto the late mode yields

$$\left|\langle 0|\hat{b}_L\hat{U}_0\hat{a}_L^\dagger|0\rangle\right|^2 = \frac{1}{4}, \tag{50}$$

while onto the early mode

$$\left|\langle 0|\hat{b}_E\hat{U}_0\hat{a}_L^\dagger|0\rangle\right|^2 = \frac{1}{4}. \tag{51}$$

Even though the photon was contained entirely in the late input mode, there is a $\frac{1}{4}$ probability of measuring it in the early mode on the transmitted side after interacting with the beam splitter. One can perform a similar calculation in projecting onto the $\hat{a}_{E,L}$ modes, yielding a total probability equal to one.

Clearly, the unitary of Eq. (5) admits solutions where superluminal signaling is possible, violating relativistic constraints (a photon can be detected outside the lightcone). This is due to the tacit assumption built into the unitary itself, which (a) neglects time ordering and thus (b) allows for the action of the mirror to occur instantaneously over a delocalized time window. This can be considered a quantum-optical example of Sorkin's well-known impossible measurement problem [33], in which instantaneous or nonlocal measurements of an observable allow for acausal information transfer between two parties. We ask, What is the consistent treatment for the propagation of temporally extended modes through such mirrors which obeys relativistic and causality considerations?

V. TELEFILTERS AND TELEMIRRORS WITH TEMPORAL-MODE INPUTS

In Sec. III we showed how continuous-variable teleportation protocols function as mode-selective telefilters and telemirrors which act on an input multimode field. The mode of interest $\hat{j}_0$ is selected by the telefilter (or telemirror) at the level of the homodyne measurement (or the generation of the classical channel), allowing it to propagate to Bob while all other modes are filtered or reflected. As the entanglement resource becomes very strong, $\hat{j}_0$ is perfectly reconstructed by Bob.

In Sec. IV we discussed how these representations of the teleportation protocols neglect the temporal aspects of the mode propagation through the circuit, under the assumption that the input modes are short in time. While these protocols obey causality [unlike the mode-selective mirrors constructed from the unitary of Eq. (5)], it is important to understand how they affect modes which are not highly localized in time. To do so, we study a series of teleportation protocols where the input field mode is distributed over two temporal modes. Using this approach allows us to explicitly investigate the action of the telemirror on an input which is delocalized in time. This can be extended to an N-mode input (Appendix D), which becomes a better approximation to a continuous spatiotemporal wave packet as $N \to \infty$. The desired operation of this temporal-mode teleporter is that a single superposition of the inputs (say, the symmetric superposition) is transmitted to the receiver, while the orthogonal superposition (the antisymmetric superposition) and all other orthogonal mode components (previously denoted by the $\hat{j}_\perp$ modes) are filtered out or reflected.

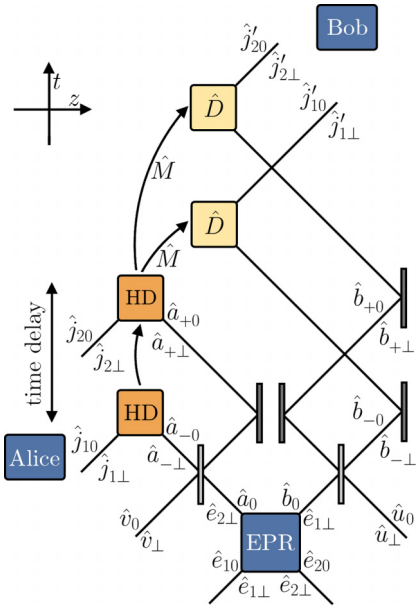

FIG. 7. Circuit diagram for the temporal-mode telefilter, which takes as inputs the temporal modes $\hat{j}_1$ and $\hat{j}_2$. The arrow connecting the two homodyne detectors signifies that the measurement results of $\hat{j}_{i0}$ are added together before displacing the $\hat{b}_{\pm 0}$ modes, respectively. The light gray mirrors are characterized by the transmission coefficient α and phase ϕ. The dark gray mirrors are non-mode-selective. The time delay between the second homodyne measurement and the displacements of $\hat{b}_{\pm 0}$ can be made arbitrarily small; however, the fundamental time delay on the mode propagation is constrained by the arrival times of the inputs $\hat{j}_1$ and $\hat{j}_2$. As previously, the $\perp$ modes are only affected by the non-mode-selective beam splitters, and note the two-mode squeezer which generates the EPR resource. Likewise, we have utilized our dual-rail representation of the light beams, within which the orthogonal 0 and $\perp$ modes copropagate.

A. Time-delayed temporal-mode telefilter

We first consider what we refer to as the temporal-mode telefilter, building off the atemporal representation of the mode-selective telefilter introduced in Sec. II. Figure 7 shows the circuit diagram. Like the previous analyses, on each rail of

the circuit the $\perp$ modes copropagate with the 0 modes, which are the set of modes which we are interested in selecting. Here our assumption is that the local oscillator modes are prepared in the same spatiotemporal mode as $\hat{j}_{10}$ and $\hat{j}_{20}$, as well as the entanglement resource modes $\hat{a}_0$ and $\hat{b}_0$.

Let us explain the protocol enacted by the temporal-mode telefilter. Just as in Fig. 2, the entangled beams $\hat{a}_0$ and $\hat{b}_0$ are sent to Alice and Bob, respectively. Since the input is distributed over two temporal modes, the entanglement resource needs to be distributed likewise. It is the choice of the entanglement mode superposition which characterizes the mode selectivity of the temporal-mode telefilter. The entanglement resource modes are distributed into two temporal modes using passive beam splitters with transmission coefficient α and phase ϕ:

$$\begin{aligned}
\hat{a}_{-0} &= \sqrt{\alpha}\hat{v}_0 - ie^{-i\phi}\sqrt{1-\alpha}\hat{a}_0,\\
\hat{a}_{+0} &= \sqrt{\alpha}\hat{a}_0 - ie^{i\phi}\sqrt{1-\alpha}\hat{v}_0,\\
\hat{b}_{-0} &= \sqrt{\alpha}\hat{u}_0 - ie^{-i\phi}\sqrt{1-\alpha}\hat{b}_0,\\
\hat{b}_{+0} &= \sqrt{\alpha}\hat{b}_0 - ie^{i\phi}\sqrt{1-\alpha}\hat{u}_0.
\end{aligned} \tag{52}$$

The $\hat{a}_{\pm\perp}$ and $\hat{b}_{\pm\perp}$ vacuum modes are constructed from parallel relations to Eq. (52), replacing the 0 modes with the copropagating $\perp$ modes. The $-$ $(+)$ nomenclature is used here to denote the early (late) mode, referring to the overlaid spacetime coordinates of Fig. 7. To perform the teleportation protocol, we perform the dual homodyne measurements explicated in Sec. III A using the inputs $\hat{j}_{10}$ and $\hat{j}_{20}$, mixed with the entanglement resource modes $\hat{a}_{\pm 0}$. This is achieved first by mixing $\hat{j}_{10}$ and $\hat{j}_{20}$ with the earlier and later parts of the entanglement resource modes, respectively,

$$\begin{aligned}
\hat{j}'_{10} &= \frac{1}{\sqrt{2}}(\hat{j}_{10} + \sqrt{\alpha}\hat{v}_0 - ie^{-i\phi}\sqrt{1-\alpha}\hat{a}_0),\\
\hat{a}'_{-0} &= \frac{1}{\sqrt{2}}(\hat{j}_{10} - \sqrt{\alpha}\hat{v}_0 + ie^{-i\phi}\sqrt{1-\alpha}\hat{a}_0),\\
\hat{j}'_{20} &= \frac{1}{\sqrt{2}}(\hat{j}_{20} + \sqrt{\alpha}\hat{a}_0 - ie^{i\phi}\sqrt{1-\alpha}\hat{v}_0),\\
\hat{a}'_{+0} &= \frac{1}{\sqrt{2}}(\hat{j}_{20} - \sqrt{\alpha}\hat{a}_0 + ie^{i\phi}\sqrt{1-\alpha}\hat{v}_0),
\end{aligned} \tag{53}$$

before coupling them with the coherently displaced local oscillator modes, detecting the photon numbers at the output ports and constructing the conjugate quadrature operators. These quadrature operators are then used to construct the measurement operators (i.e., the classical measurement result) of the form

$$\begin{aligned}
\hat{M}_1 &= \hat{X}_{\hat{j}'_{10}} + i\hat{P}_{\hat{a}_{-0}}, \quad \hat{M}_2 = \hat{X}_{\hat{j}'_{20}} + i\hat{P}_{\hat{a}_{+0}},\\
\hat{M}_1 &= \hat{X}_{\hat{a}_{-0}} + i\hat{P}_{\hat{j}'_{10}}, \quad \hat{M}_2 = \hat{X}_{\hat{a}_{+0}} + i\hat{P}_{\hat{j}'_{20}}.
\end{aligned} \tag{54}$$

Now recall that we are treating $\hat{j}_{10}$ and $\hat{j}_{20}$ as the individual temporal components of a single input wave-packet mode to be selected by the teleporter. To successfully enact the teleportation of this wave packet, one has to combine the local measurement results from each of the temporal modes and then use this to displace Bob's side of the entanglement resource $\hat{b}_{\pm 0}$. Clearly, one cannot perform a measurement of $\hat{j}_{20}$ before it has entered the apparatus; nor can the entire mode be teleported before $\hat{j}_{20}$ has been measured. This constraint time orders the two independent measurement processes in the circuit, preventing $\hat{j}_{20}$ from being teleported before $\hat{j}_{10}$. To emphasize this point, one should consider Fig. 7 as occurring on a flat background with spacetime coordinates (t, z) (as shown at the top of the figure) where the rails in the circuit now represent the lightlike propagation of the modes.

Returning to the measurement, we can construct a total measurement operator $\hat{M}$ as a linear combination of the individual results

$$\hat{M} = \zeta_1(\alpha,\phi)\hat{M}_1 + \zeta_2(\alpha,\phi)\hat{M}_2, \tag{55}$$

where $\zeta_i(\alpha,\phi) \in \mathbb{C}$. This summation over the measurement results is indicated by the arrow connecting the two homodyne measurements in the circuit of Fig. 7. The total measurement operator is communicated classically to Bob (similarly depicted as arrows), which he uses to displace his part of the distributed entanglement resource modes $\hat{b}_{\pm 0}$. He obtains the output modes

$$\hat{j}'_{10} = \hat{b}_{-0} + \lambda_1(\alpha,\phi)\hat{M}, \tag{56}$$

$$\hat{j}'_{20} = \hat{b}_{+0} + \lambda_2(\alpha,\phi)\hat{M}, \tag{57}$$

where $\lambda_i(\alpha,\phi) \in \mathbb{C}$. As we show in Appendix C, Alice can select any arbitrary superposition of the inputs $\hat{j}_{i0}$ by tuning the physical properties of the optical elements and the homodyne measurements.

Let us consider a simple case. In our construction, the phase of the quadrature operators in the measurement process, the distribution of the entanglement resource, and the magnitude of the displacements made to Bob's side of the entanglement resource modes completely determine the properties of the mode to be selected. The most straightforward example is obtained by taking the $\hat{X}_{a_{\pm 0}}$ and $\hat{P}_{j'_{i0}}$ quadratures at the homodyne measurement and distributing $\hat{a}_{\pm 0}$ and $\hat{b}_{\pm 0}$ equally between the early and late temporal modes. In such a case, the transmitted mode will be a balanced superposition of the inputs $\hat{j}_{10}$ and $\hat{j}_{20}$. Taking, for example, $\alpha = \frac{1}{2}$, $\phi = -\pi/2$, and the measurement results

$$\hat{M}_1 = |\beta|\big(\hat{X}_{a_{-0}} + i\hat{P}_{j'_{10}}\big) = |\beta|(\sqrt{2}\hat{j}_{10} - \hat{a}_0^\dagger - \hat{v}_0^\dagger), \tag{58}$$

$$\hat{M}_2 = |\beta|\big(\hat{X}_{a_{+0}} + i\hat{P}_{j'_{20}}\big) = |\beta|(\sqrt{2}\hat{j}_{20} - \hat{a}_0^\dagger + \hat{v}_0^\dagger), \tag{59}$$

we obtain, for the total measurement operator,

$$\hat{M} = \frac{1}{\sqrt{2}}(\hat{j}_{10} + \hat{j}_{20} - \sqrt{2}\hat{a}_0^\dagger), \tag{60}$$

having taken $\zeta_i(\alpha,\phi) = 1/2\sqrt{2}|\beta|$, which achieves a unity gain channel between Alice and Bob. Bob then displaces his part of the distributed entanglement $\hat{b}_{\pm 0}$ with the total measurement operator to obtain the outputs

$$\hat{j}'_{10} = \frac{1}{2}(\hat{j}_{10} + \hat{j}_{20}) + \frac{1}{\sqrt{2}}(\hat{b}_0 - \hat{a}_0^\dagger) + \frac{1}{\sqrt{2}}\hat{u}_0, \tag{61}$$

$$\hat{j}'_{20} = \frac{1}{2}(\hat{j}_{10} + \hat{j}_{20}) + \frac{1}{\sqrt{2}}(\hat{b}_0 - \hat{a}_0^\dagger) - \frac{1}{\sqrt{2}}\hat{u}_0, \tag{62}$$

where we have taken $\lambda_i(\alpha,\phi)=1$, while the copropagating $\perp$ modes are $\hat{j}'_{1\perp}=\hat{b}_{-\perp}$ and $\hat{j}'_{2\perp}=\hat{b}_{+\perp}$, which are superpositions of $\hat{e}_{1\perp}$ and $\hat{u}_{\perp}$, respectively, defined analogously to Eq. (52). These can be mixed back together on a balanced beam splitter to retrieve the input vacuum modes:

$$\hat{o}^{(l)}_{1\perp}=\frac{1}{\sqrt{2}}(\hat{j}'_{2\perp}+\hat{j}'_{1\perp})=\hat{e}_{1\perp}, \tag{63}$$

$$\hat{o}^{(r)}_{1\perp}=\frac{1}{\sqrt{2}}(\hat{j}'_{1\perp}-\hat{j}'_{2\perp})=\hat{u}_{1\perp}. \tag{64}$$

Meanwhile, for the 0 modes, we can likewise mix the outputs on a balanced beam splitter, yielding

$$\begin{aligned}\hat{o}^{(l)}_{10}&=\frac{1}{\sqrt{2}}(\hat{j}'_{20}+\hat{j}'_{10})\\&=\frac{1}{\sqrt{2}}(\hat{j}_{10}+\hat{j}_{20})+(\hat{b}_0-\hat{a}^{\dagger}_0),\end{aligned} \tag{65}$$

$$\hat{o}^{(r)}_{10}=\frac{1}{\sqrt{2}}(\hat{j}'_{10}-\hat{j}'_{20})=\hat{u}_0. \tag{66}$$

We find that the symmetric superposition of the input temporal modes has been successfully teleported to $\hat{o}^{(l)}_{10}$ along with the entanglement resource modes, while the vacuum beam-splitter input $\hat{u}_0$ is isolated to the other output $\hat{o}^{(r)}_{10}$. We conclude that the device successfully selects the mode of interest, i.e., only one temporal superposition is transmitted, while the orthogonal superposition is filtered out at the level of the measurement. All modes which appear at Bob's output are in the vacuum. In Appendix C we show how through an appropriate choice of the quadrature phases and the beam-splitter coefficients, Alice can select any arbitrary superposition mode to be transmitted to Bob.

Despite the success of our model in functioning mode selectively, Fig. 7 also reveals that this mode selectivity cannot be achieved without a time delay which minimally matches the length of the input field mode. In our simplified two-mode case, the temporal length of the input wave packet is simply the time delay between modes $\hat{j}_{10}$ and $\hat{j}_{20}$. For teleportation to successfully occur, the individual local measurements enacted upon the input temporal modes must be coherently combined (added together) *and then* used to displace Bob's side of the entanglement. Necessarily then, Alice must wait until the entire wave packet (i.e., both the earlier and later temporal components) has been measured, before sending the classical channel to Bob. Note once more that the atemporal representation of the telefilter protocol from Sec. III obeys this time delay, but such a feature cannot be discerned unless treating the input modes as we have done here. One may be relieved that such a delay exists, meaning that the causality-violating scenario of Fig. 6(b) is not generally permitted. If one could enact the homodyne measurement of the entire wave packet instantaneously, there would be no time delay. However, such a scenario is unphysical and will inevitably lead to situations in which the input mode is teleported to an output mode which is earlier in time.

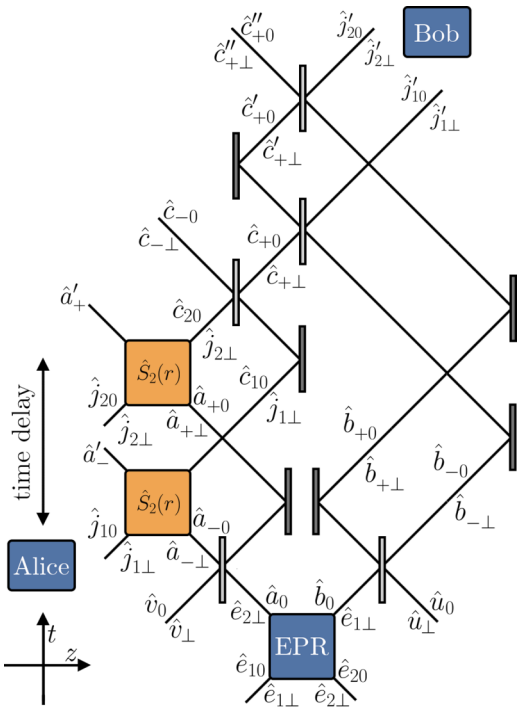

FIG. 8. Circuit diagram for the temporal-mode telemirror. The homodyne measurements are replaced by two-mode squeezing and the coherent displacements are replaced by beam-splitter interactions between the classical channel modes and the $\hat{b}_{\pm 0}$ modes. Note that the modes $\hat{a}'_{\pm}$ really contain $\hat{a}'_{\pm 0}$ and $\hat{a}_{\pm\perp}$, where the latter are not affected by the two mode squeezers $\hat{S}_2(r)$. We have not displayed these for aesthetic reasons.

B. Time-delayed temporal-mode telemirror

We now consider the all-optical version of the mode-selective telemirror with two input temporal modes, shown schematically in Fig. 8. This approach is fully unitary and also allows us to calculate both the transmitted and reflected modes. As with the temporal-mode telefilter, the entanglement resource modes are distributed into spatial superpositions [Eq. (52)]. Rather than mixing the entanglement with the input temporal modes and performing a homodyne measurement, the classical channel is enacted via two-mode squeezing,

$$\hat{c}_{10}=\cosh(r)\hat{j}_{10}+\sinh(r)\hat{a}^{\dagger}_{-0}, \tag{67}$$

$$\hat{c}_{20}=\cosh(r)\hat{j}_{20}+\sinh(r)\hat{a}^{\dagger}_{+0}, \tag{68}$$

while the other ports propagate to the reflected side:[2]

$$\hat{a}'_{-0}=\cosh(r)\hat{a}_{-0}+\sinh(r)\hat{j}^{\dagger}_{10}, \tag{69}$$

$$\hat{a}'_{+0}=\cosh(r)\hat{a}_{+0}+\sinh(r)\hat{j}^{\dagger}_{20}. \tag{70}$$

As with the atemporal representation of the telefilter and telemirror, Eqs. (67) and (68) are identical to the measurement operators in Eqs. (58) and (59) modulo some squeezing phase between $\hat{j}_{i0}$ and $\hat{a}_{\pm 0}$, in the limit of high gain (i.e., $r\gg 1$ for the telemirror and $|\beta|\gg 1$ in the telefilter). As usual, we

[2]The $\perp$ modes $\hat{a}_{\pm\perp}$ are unaffected by the squeezer.

assume that only the 0 modes and the associated entanglement resource modes are mode matched to the squeezers generating the classical channel. The $\hat{c}_{i0}$ modes are highly amplified by the two-mode squeezers $\hat{S}_2(r)$ and can thus be regarded as good approximations to a classical field while the $\perp$ modes remain unaffected by the squeezers.

In the temporal-mode telefilter, the individual measurement results are added together and used to displace the earlier and later components of Bob's entanglement resource mode $\hat{b}_{\pm 0}$. The equivalent operation in the all-optical version of the protocol is to mix the classical channel modes on a passive beam splitter to obtain an analogous total measurement operator. We have

$$\hat{c}_{-0} = \sqrt{\alpha}\hat{c}_{10} - ie^{i\phi_{c_0}}\sqrt{1-\alpha}\hat{c}_{20}, \tag{71}$$

$$\hat{c}_{+0} = \sqrt{\alpha}\hat{c}_{20} - ie^{-i\phi_{c_0}}\sqrt{1-\alpha}\hat{c}_{10}, \tag{72}$$

where ϕ_{c_0} is the beam-splitter phase. The $+$ part of this mode is likewise used to displace one of the temporal entanglement resource modes on Bob's side,

$$\hat{j}'_{10} = \sqrt{\eta_-}\hat{b}_{-0} - ie^{-i\phi_-}\sqrt{1-\eta_-}\hat{c}_{+0}, \tag{73}$$

$$\hat{c}'_{+0} = \sqrt{\eta_-}\hat{c}_{+0} - ie^{i\phi_-}\sqrt{1-\eta_-}\hat{b}_{-0}, \tag{74}$$

while the leftover part of the channel is used to displace the later temporal entanglement resource mode:

$$\hat{j}'_{20} = \sqrt{\eta_+}\hat{b}_{+0} - ie^{-i\phi_+}\sqrt{1-\eta_+}\hat{c}'_{+0}, \tag{75}$$

$$\hat{c}''_{+0} = \sqrt{\eta_+}\hat{c}'_{+0} - ie^{i\phi_+}\sqrt{1-\eta_+}\hat{b}_{+0}. \tag{76}$$

Here $\phi_\pm$ are variable beam-splitter phases. Let us show how to select the symmetric superposition of $\hat{j}_{i0}$. First, let us take $\phi = \phi_\pm = -\pi/2$ and $\phi_{c_0} = \pi/2$ with the beam-splitter transmission coefficients

$$\eta_\pm = 1 - \frac{1}{2\cosh^2(r)}. \tag{77}$$

We have chosen $\eta_\pm$ so that most of the highly amplified channel is reflected away from the output; in the limit of high gain, this ensures that the entanglement resource modes are transmitted to the output modes. The output modes (in the limit $r \to \infty$) are given by

$$\hat{j}'_{10} = -\frac{1}{2}(\hat{j}_{10} + \hat{j}_{20}) + \frac{1}{\sqrt{2}}(\hat{b}_0 - \hat{a}_0^\dagger) + \frac{1}{\sqrt{2}}\hat{u}_0, \tag{78}$$

$$\hat{j}'_{20} = -\frac{1}{2}(\hat{j}_{10} + \hat{j}_{20}) + \frac{1}{\sqrt{2}}(\hat{b}_0 - \hat{a}_0^\dagger) - \frac{1}{\sqrt{2}}\hat{u}_0. \tag{79}$$

The symmetric superposition of $\hat{j}_{i0}$ and the entanglement resource modes are transmitted to both output ports, along with an extra vacuum mode used to distribute the entanglement across two temporal modes. Mixing these finally on a balanced beam splitter yields

$$\hat{o}^{(l)}_{10} = \frac{1}{\sqrt{2}}(\hat{j}'_{20} + \hat{j}'_{10}) = -\frac{1}{\sqrt{2}}(\hat{j}_{10} + \hat{j}_{20}) + (\hat{b}_0 - \hat{a}_0^\dagger), \tag{80}$$

$$\hat{o}^{(r)}_{10} = \frac{1}{\sqrt{2}}(\hat{j}'_{10} - \hat{j}'_{20}) = \hat{u}_0, \tag{81}$$

which is just the symmetric superposition of $\hat{j}_{10}$ and $\hat{j}_{20}$ modulo a global phase, carrying with it the entanglement resource modes, and vacuum in the other. This result is analogous to that found in Eq. (66), where the mode of interest (the symmetric superposition, determined by the beam-splitter settings) is retrieved at one of the output ports, while the other mode merely contains the $\hat{u}_0$ mode coming from the beam-splitter mixing. This further illustrates how the telefilter and the unitary telemirror are equivalent in the transformations they enact on the selected mode as it is transmitted through the circuit. As we demonstrate in Appendix C, Alice can select any arbitrary superposition of $\hat{j}_{i0}$ by tuning the beam-splitter coefficients appropriately.

We can also calculate the output reflected modes. Following a straightforward calculation in Appendix A, the vacuum modes used to create the temporal superposition $\hat{v}_0$ as well as the entanglement resource modes $\hat{e}_{10}$ and $\hat{e}_{20}$ are constructed on the reflected side. More importantly, the modes

$$\frac{1}{\sqrt{2}}(\hat{j}_{10} - \hat{j}_{20}), \tag{82}$$

$$\frac{1}{\sqrt{2}}(\hat{j}_{1\perp} + \hat{j}_{2\perp}), \tag{83}$$

$$\frac{1}{\sqrt{2}}(\hat{j}_{1\perp} - \hat{j}_{2\perp}), \tag{84}$$

which are mutually orthogonal to the transmitted symmetric superposition, are also reflected.

What about the other $\perp$ modes? Recall that these modes are unaffected by the two-mode squeezers $\hat{S}_2(r)$, while they are affected by the non-mode-selective beam splitters. By straightforwardly tracing the propagation of these modes through the circuit, we find that the $\perp$ modes at Bob's side are given by $\hat{o}^{(l)}_{1\perp} = \hat{u}_{1\perp}$ and $\hat{o}^{(r)}_{1\perp} = \hat{e}_{1\perp}$,[3] which are simply vacuum modes involved in the entanglement generation, while the remaining $\perp$ vacuum modes are retrieved on the reflected side: $\hat{e}_{2\perp}$ and $\hat{v}_\perp$.

The all-optical telemirror nicely illustrates the necessity of the time delay as the input temporal modes pass through the circuit. From Fig. 8, a fundamental time delay is imposed on the teleportation of the temporal modes, since the channels must be combined to form the equivalent of the total measurement operator $\hat{c}_{+0}/\hat{c}'_{+0}$. This delay is a function of the temporal length of the mode itself, in our model, the time delay between the arrival of the input pulses $\hat{j}_{10}$ and $\hat{j}_{20}$. As in the temporal-mode telefilter, this constraint ensures the preservation of causality by time ordering the unitary operators so that they act on the input modes in a consistent temporal order. This prevents a photon prepared in the late mode $\hat{j}_{20}$ from arriving earlier than it was sent.

VI. TEMPORAL-MODE TELEPORTERS WITH NO TIME DELAY

The protocols studied in Sec. III demonstrate that, in general, mode-selective quantum-optical mirrors enact an unavoidable and intrinsic time delay on the propagation of

[3]We utilize the definitions of $\hat{o}^{(l,r)}_{1\perp}$ shown in Eqs. (63) and (64).

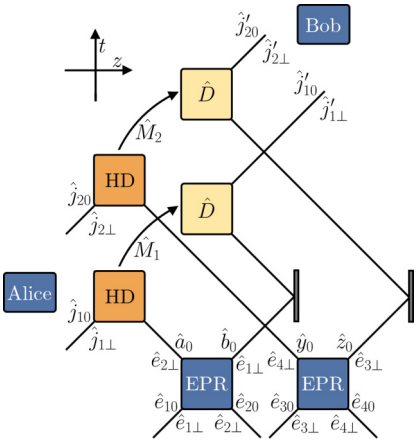

FIG. 9. Circuit diagram for the no-delay telefilter with independent entanglement resources. Here $\hat{y}_0$ and $\hat{z}_0$ represent the entanglement resource modes used to teleport $\hat{j}_{20}$. These are constructed from the vacuum inputs $\hat{e}_{30}$ and $\hat{e}_{40}$.

input temporal modes. Such an effect was not observed in the original CV teleportation protocols because the temporal dimension of the input modes was neglected. This is akin to neglecting time-ordering effects in the original unitary for the mode-selective beam splitter [Eq. (5)].

Nevertheless, our results beg the question of what goes wrong if we try to construct a mode-selective mirror interaction which does not induce an intrinsic time delay. Rather than integrating over the entire temporal length of the mode (e.g., waiting to combine the measurement results on the individual modes together), our next models consider the teleportation of the individual temporal modes separately and continuously before coherently recombining them at the output. We study two approaches: In the first, there are two independent entanglement resources for each of the temporal modes, while in the second, we distribute the entanglement resource modes into earlier and later components, as was done for the temporal-mode teleporters introduced previously. For simplicity, we will just consider the selection of an equal symmetric superposition and the filtering or reflection of its antisymmetric pair.

A. Teleportation with independent entanglement resources

Our first approach to circumventing the time delay is shown in Fig. 9. As before, we utilize homodyne measurements to obtain the results $\hat{M}_i$, which represent the classical channel connecting Alice and Bob. Alice performs the individual measurements separately and sends them continuously to Bob as she obtains them. This avoids the fundamental time delay introduced in the temporal-mode telefilter and telemirror.

It is straightforwardly shown that the output of the circuit is identical to the homodyne measurement telefilter, but now teleports both temporal modes

$$\hat{j}'_{10} = \hat{j}_{10} + (\hat{b}_0 - \hat{a}_0^\dagger), \quad \hat{j}'_{20} = \hat{j}_{20} + (\hat{y}_0 - \hat{z}_0^\dagger),$$
$$\hat{j}'_{1\perp} = \hat{e}_{1\perp}, \quad \hat{j}'_{2\perp} = \hat{e}_{3\perp}, \tag{85}$$

where $\hat{y}_0$ and $\hat{z}_0$ are generated by two-mode squeezing of independent vacuum inputs. The other vacuum inputs $\hat{e}_{2\perp}$ and

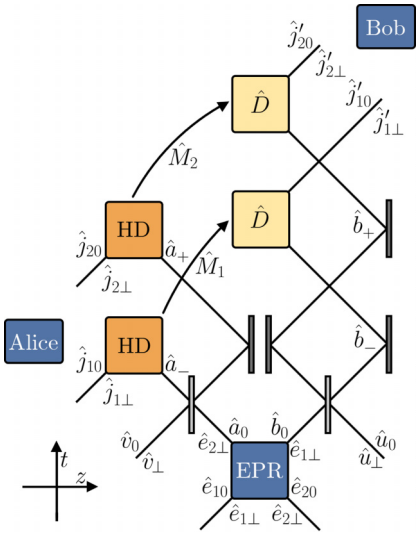

FIG. 10. Circuit diagram for the no-delay telefilter. The $\hat{a}_\pm$ and $\hat{b}_\pm$ should be understood as containing the orthogonal copropagating 0 and $\perp$ modes (we have not displayed these components for aesthetic reasons).

$\hat{e}_{4\perp}$ are filtered out at the homodyne measurement. In the limit of perfect entanglement between $\hat{b}_0$ and $\hat{a}_0$ and between $\hat{y}_0$ and $\hat{z}_0$, the $\hat{j}_{i0}$ modes are individually recovered at the outputs. This of course presents an immediate and obvious issue: Any temporal superposition of $\hat{j}_{i0}$, in addition to its orthogonal complement, can be reconstructed by Bob. For example,

$$\hat{o}_{10}^{(l)} = \frac{1}{\sqrt{2}}(\hat{j}'_{10} + \hat{j}'_{20}) = \frac{1}{\sqrt{2}}(\hat{j}_{10} + \hat{j}_{20}), \tag{86}$$
$$\hat{o}_{10}^{(r)} = \frac{1}{\sqrt{2}}(\hat{j}'_{10} - \hat{j}'_{20}) = \frac{1}{\sqrt{2}}(\hat{j}_{10} - \hat{j}_{20}). \tag{87}$$

Thus, while the time delay on the propagation of the input modes is avoided, the introduction of two separate entanglement resource mode pairs means that the protocol ultimately fails to be mode selective. Nor can it be considered mode discriminating, because all superpositions with temporal support on $\hat{j}_{i0}$ are teleported ideally.

B. No-delay temporal-mode telefilter

Instead of utilizing independent entanglement resources, we now take the previous approach by distributing a single entanglement resource over two temporal modes. Our proposed circuit for this model, which we refer to as the no-delay telefilter, is displayed in Fig. 10. As usual, homodyne measurements are enacted by mode matching the entanglement resource mode with the input mode and local oscillator to obtain the classical results $\hat{M}_i$. Unlike the previous model, where Alice would add the measurement results of both modes together (requiring her to wait until both $\hat{j}_{10}$ and $\hat{j}_{20}$ had entered the apparatus), Alice sends the individual measurement results $\hat{M}_1$ and $\hat{M}_2$ to Bob on the fly.

Alice and Bob distribute the entanglement resource modes in a superposition of earlier and later components. Let us

consider the same beam-splitter settings as Sec. V A. Using again the measurement results

$$\hat{M}_1 = |\beta|(\hat{X}_{a_{-0}} + i\hat{P}_{j'_{10}}) = |\beta|(\sqrt{2}\hat{j}_{10} - \hat{a}_0^\dagger - \hat{v}_0^\dagger), \quad (88)$$

$$\hat{M}_2 = |\beta|(\hat{X}_{a_{+0}} + i\hat{P}_{j'_{20}}) = |\beta|(\sqrt{2}\hat{j}_{20} - \hat{a}_0^\dagger + \hat{v}_0^\dagger), \quad (89)$$

Bob displaces the individual modes $\hat{b}_{\pm 0}$ to obtain the outputs

$$\hat{j}'_{10} = \hat{j}_{10} + \frac{1}{\sqrt{2}}(\hat{b}_0 - \hat{a}_0^\dagger) + \frac{1}{\sqrt{2}}(\hat{u}_0 - \hat{v}_0^\dagger), \quad (90)$$

$$\hat{j}'_{20} = \hat{j}_{20} + \frac{1}{\sqrt{2}}(\hat{b}_0 - \hat{a}_0^\dagger) - \frac{1}{\sqrt{2}}(\hat{u}_0 - \hat{v}_0^\dagger), \quad (91)$$

where we have used $\zeta_i = 1/\sqrt{2}|\beta|$ to achieve a unity gain channel for the individual temporal components. As can be seen, the earlier and later input modes are teleported to the earlier and later output modes, respectively, with two sources of additional noise from the beam-splitter inputs. Mixing the output modes back together on a balanced beam splitter yields

$$\hat{o}_{10}^{(l)} = \frac{1}{\sqrt{2}}(\hat{j}_{10} + \hat{j}_{20}) + (\hat{b}_0 - \hat{a}_0^\dagger), \quad (92)$$

$$\hat{o}_{10}^{(r)} = \frac{1}{\sqrt{2}}(\hat{j}_{10} - \hat{j}_{20}) + (\hat{u}_0 - v_0^\dagger). \quad (93)$$

Similar to teleportation with independent entanglement resources, both the symmetric and antisymmetric superpositions are transmitted to Bob. The difference is that the symmetric superposition has been teleported along with the entanglement resource modes, while the antisymmetric superposition has been teleported with additional noise from the beam-splitter inputs. As such, this second model for the no-delay telefilter exhibits a kind of mode-discriminating property. Rather than uniquely affecting a single mode and transmitting all others through the identity channel, the converse is true; the selected mode is transmitted without change, while the orthogonal mode is polluted by noise. Furthermore, in the limit where these extraneous modes are highly noisy, any signal encoded in the antisymmetric superposition mode cannot be detected by Bob, as it is buried within this noise. This could be achieved if, for example, $\hat{u}_0$ and $\hat{v}_0$ are generated from independent entanglement sources, where the other half of the entangled pairs are sent to the reflected side of the mirror. Bob, on the receiving side of the mirror, traces out these reflected modes and thus cannot purify $\hat{o}_{10}^{(r)}$ to retrieve the orthogonal mode. As shown in Appendix C, one can tune the beam-splitter coefficients appropriately so that any specified superposition of the temporal modes $\hat{j}_{i0}$ can be transmitted along with the entanglement resource and thus be discriminated from its orthogonal superposition mode which carries the additional noise.

Why do violations of causality not occur in the no-delay telefilter? Suppose we prepare a mode $\hat{i}$ in a single-photon state in a localized time-bin mode prior to the input temporal modes $\hat{j}_{10}$ and $\hat{j}_{20}$ (see Fig. 11). We note that this input could be in some arbitrary state, but using a single photon is conceptually straightforward. From Eqs. (90) and (91) one sees that if a photon is prepared in the late mode $\hat{j}_{20}$, it cannot be transmitted to the early mode $\hat{j}'_{10}$. Nor can the converse

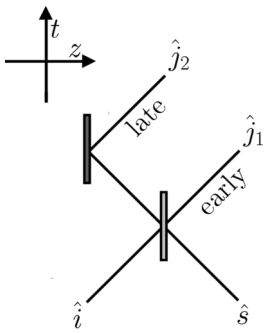

FIG. 11. Schematic diagram of the input modes, split into a superposition of early and late time bins $\hat{j}_{10}$ and $\hat{j}_{20}$ at a beam splitter. Here $\hat{i}$ could be prepared in a single-photon state, while $\hat{s}$ is in the vacuum.

be true: A photon prepared in the early mode $\hat{j}_{10}$ cannot be transmitted to the late mode $\hat{j}'_{20}$. Causality is manifestly preserved.

Alternatively, one may ask what information about the photon arrival time can be obtained by Bob. If he makes (photon number) measurements in the symmetric superposition basis, he will detect the single photon half of the time. This is expected if the photon is initially prepared in either of the early or late temporal modes. To perform such a measurement, he requires an additional time delay (to recombine the outputs $\hat{j}'_{i0}$ together) so that the entire mode can be measured. On the other hand, Bob may attempt to determine whether the photon arrived in the early or late output temporal mode [see Eqs. (90) and (91) and Fig. 10]. However, such an attempt will be limited by the presence of unavoidable excess noise on both the early and late modes that is only canceled if the correct temporal-mode superposition is detected. Indeed, injecting additional noise at $\hat{u}_0$ and $\hat{v}_0$ could effectively erase all information carried by any modes other than the correct temporal-mode superposition. That is, the only mode that is cleanly transmitted is the selected mode; all others are polluted with noise. In this sense the device in this section achieves mode discrimination (i.e., a limited kind of mode selectivity), with no temporal delay, while still being causal.

C. No-delay temporal-mode telemirror

For completeness, in this section we provide a brief discussion of the no-delay temporal-mode telemirror (see Fig. 12). The full calculation of the input-output relations is shown in Appendix C. As usual, the entanglement resource is distributed into early and late temporal modes, which interact with the input temporal modes at two-mode squeezers, generating the classical channel. Like the temporal-mode telefilter, the individual channels are mixed with Bob's half of the entanglement resource modes, from which he recovers as outputs (choosing an equal distribution of the entanglement resource and appropriate beam-splitter phases)

$$\hat{j}'_{10} = \hat{j}_{10} - \frac{\tanh(r)}{\sqrt{2}}(\hat{b}_0 - \hat{a}_0^\dagger) - \frac{\tanh(r)}{\sqrt{2}}(\hat{u}_0 - \hat{v}_0^\dagger), \quad (94)$$

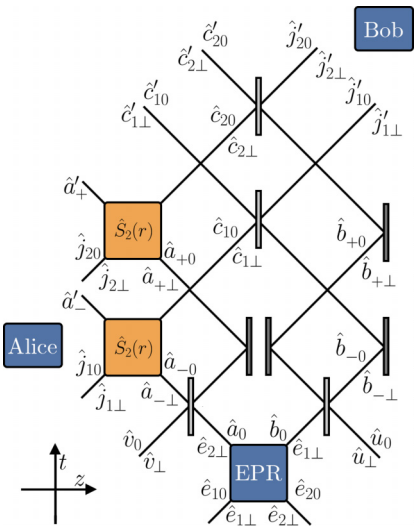

FIG. 12. Circuit diagram of the no-delay temporal-mode telemirror. The modes $\hat{a}_{\pm 0}$, $\hat{a}_{\pm\perp}$, $\hat{b}_{\pm 0}$, and $\hat{b}_{\pm\perp}$ are defined in Eq. (52). Likewise the classical channel modes $\hat{c}_{i0}$ and $\hat{c}_{i\perp}$ are defined in Eqs. (67) and (68).

$$\hat{j}'_{20} = \hat{j}_{20} - \frac{\tanh(r)}{\sqrt{2}}(\hat{b}_0 - \hat{a}_0^\dagger) + \frac{\tanh(r)}{\sqrt{2}}(\hat{u}_0 - \hat{v}_0^\dagger). \quad (95)$$

Equations (94) and (95) are analogous to Eqs. (90) and (91) obtained for the no-time-delay telefilter (modulo arbitrarily chosen phase factors). After mixing the modes together, one of the outputs perfectly teleports the symmetric superposition of $\hat{j}_{10}$ and $\hat{j}_{20}$, while the other teleports the antisymmetric superposition classically, with the additional noise source:

$$\hat{o}_{10}^{(l)} = \frac{1}{\sqrt{2}}(\hat{j}_{10} + \hat{j}_{20}) - \tanh(r)(\hat{b}_0 - \hat{a}_0^\dagger), \quad (96)$$

$$\hat{o}_{10}^{(r)} = \frac{1}{\sqrt{2}}(\hat{j}_{10} - \hat{j}_{20}) - \tanh(r)(\hat{u}_0 - \hat{v}_0^\dagger). \quad (97)$$

In the regime where this noise is very large, the no-delay telemirror is thus mode discriminating but not mode selective; one mode arrives cleanly at Bob's output (letting the entanglement resource to be very strong), while the other is polluted by noise. In Appendix C we show how Alice can discriminate any arbitrary superposition mode (i.e., teleport it along with the entanglement resource) while polluting its orthogonal complement with noise. Meanwhile, the transmitted $\perp$ modes in the limit of high gain retrieve the vacuum inputs used to perform the teleportation, $\hat{o}_{1\perp}^{(l)} = -\hat{e}_{1\perp}$ and $\hat{o}_{1\perp}^{(r)} = -\hat{u}_{1\perp}$.[4]

For the reflected modes, we retrieve, in the limit of high gain, the modes

$$\frac{1}{2\sqrt{2}}(\hat{j}_{10}^\dagger - \hat{j}_{20}^\dagger) - \hat{u}_0^\dagger + \frac{3}{2}\hat{v}_0,$$

$$\frac{1}{2\sqrt{2}}(\hat{j}_{10} - \hat{j}_{20}) + \hat{u}_0 - \frac{1}{2}\hat{v}_0^\dagger,$$

$$\frac{1}{2\sqrt{2}}(\hat{j}_{10}^\dagger + \hat{j}_{20}^\dagger) + \frac{3}{2}\hat{a}_0 - \hat{b}_0^\dagger,$$

$$\frac{1}{2\sqrt{2}}(\hat{j}_{10} + \hat{j}_{20}) - \frac{1}{2}\hat{a}_0^\dagger + \hat{b}_0. \quad (98)$$

The antisymmetric superposition appears on the reflected side with additional noise from the vacuum inputs, while the symmetric superposition becomes buried beneath the noise from the entanglement resource modes with unbalanced coefficients. In the $\perp$ modes, the leftover input vacuum modes are retrieved on the reflected side as well: $\hat{e}_{2\perp}$, $\hat{v}_{1\perp}$, $\hat{j}_{1\perp}$, and $\hat{j}_{2\perp}$.

The results from this section have affirmed those derived in Sec. V, namely, that time delays are a fundamental property of mode-selective mirrors. In particular, we attempted to circumvent this issue by transmitting (i.e., teleporting) each temporal component of the multimode input on the fly, that is, teleporting the temporal components independently, rather than waiting for the whole mode to enter the circuit. While this approach respects relativistic constraints (the propagation time of the mode is limited by the speed of light and causality is preserved), it nevertheless fails as a completely mode-selective device. This property may be problematic in scenarios where one wishes to isolate a single mode for experimental purposes or in quantum causality problems [53,54].

VII. CONCLUSION

The aim of this paper has been threefold. First, we proposed a teleportation model for the mode-selective mirror, which is widely used in quantum information and communication [4–6], relativistic quantum field theory (QFT) [9–14], and experimental applications in quantum optics [15–18].

Next we applied our model to study in detail a well-known causality problem in the propagation of temporally extended modes through such mirrors. This was motivated by our demonstration that standard treatments of the mode-selective mirror, in particular Eq. (5), can yield causality-violating results. Specifically, we showed that mode-selective mirrors necessarily delay incoming modes based on the length of the mode itself. The underlying explanation of our result is closely connected with the pathological issues arising from instantaneous nonlocal measurements in relativistic QFT [33], which have been shown to elicit violations of causality when treated without care [35]. Finally, we investigated the issues which arise when one attempts to construct a mode-selective mirror with no time delay. For such a mirror, only the selected mode is cleanly teleported. All other modes are teleported but are polluted with noise; in this sense, the mirror is mode discriminating. Furthermore, an observer on the receiving side of the mirror cannot retrieve useful information about the arrival time of a photon prepared by Alice, due to additional copropagating noise.

Our approach to mode-selective teleportation opens several pathways for future research. It first presents a method of enacting a mode-selective identity channel in quantum optics, where the prevailing techniques have been the quantum pulse gate and Raman quantum memory [15,20]. Achieving high efficiencies is a perpetual aim within the field of experimental quantum optics [16,55–57], and our approach provides a

[4]We utilize the definitions of $\hat{o}_{1\perp}^{(l,r)}$ shown in Eqs. (63) and (64).

feasible path towards this end by using well-developed techniques, e.g., homodyne detection (see also Appendix B for a discussion of the transmission efficiencies of the telefilter and telemirror). A related immediate extension to the present work would be to apply the time-bin model to the study of other mode-selective elements.

The telemirror also links quantum optics and quantum communication with the study of causality in relativistic quantum information [58] and quantum field theory. We have illuminated in a remarkably simple way the inherent issues underlying impossible measurements [33] in relativistic quantum field theory. While other works in this field have utilized theoretical techniques ranging from algebraic QFT [36] to measurement theory [35], our approach frames these effects in quantum-optical settings which have already been shown to be experimentally accessible.

ACKNOWLEDGMENTS

The authors thank Fabio Costa for fruitful discussions. This research was supported by the Australian Research Council Centre of Excellence for Quantum Computation and Communication Technology (Project No. CE170100012) and Australian Research Council Discovery Early Career Researcher Award (Grant No. DE180101443).

APPENDIX A: REFLECTED MODE FOR TELEMIRRORS

1. Mode-selective telemirror

In this Appendix we derive the unitary transformation required to retrieve the input vacuum modes $\hat{e}_{10}$ and $\hat{e}_{20}$ on the reflected side of the mode-selective (atemporal) telemirror from Sec. III C. As will be shown, these operations may be reduced to a single inverse squeezing operation, shown in Fig. 13. To derive the squeezing parameter k, it is instructive to decompose the single unitary operator $\hat{S}_2^{-1}(k)$ into a series of squeezers which reverse the initial operations performed on the input modes which generated (a) the entanglement resource modes and (b) the classical channel. Recall that the output of the classical channel squeezer and the output of the beam-splitter displacement at Bob's output port are given, respectively, by

$$\hat{a}_0' = \cosh(r)\hat{a}_0 + \sinh(r)\hat{j}_0^\dagger, \tag{A1}$$

$$\hat{c}_0' = \operatorname{sech}(r)\hat{b}_0 + \tanh(r)\cosh(r)\hat{j}_0 + \tanh(r)\sinh(r)\hat{a}_0^\dagger. \tag{A2}$$

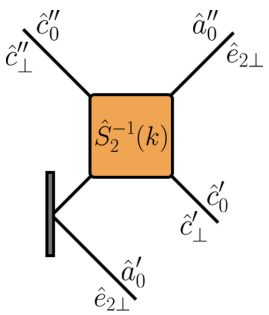

FIG. 13. Circuit diagram for the operations enacted upon the reflected modes to retrieve the input vacua for the atemporal-mode-selective telemirror.

We perform successive inverse squeezing operations on the output modes with respect to the parameters r and s used to generate the initial states

$$\hat{q}_{10} = \cosh(r)\hat{a}_0' - \sinh(r)\hat{c}_0'^\dagger, \tag{A3}$$

$$\hat{q}_{20} = \cosh(r)\hat{c}_0' - \sinh(r)\hat{a}_0'^\dagger \tag{A4}$$

and then

$$\hat{p}_{10} = \cosh(s)\hat{q}_{10} - \sinh(s)\hat{q}_{20}^\dagger, \tag{A5}$$

$$\hat{p}_{20} = \cosh(s)\hat{q}_{20} - \sinh(s)\hat{q}_{10}^\dagger. \tag{A6}$$

In the limit where $s, r \to \infty$, the reflected output modes reduce to

$$\hat{p}_{10} = \tfrac{5}{4}\hat{e}_{10} - \tfrac{3}{4}\hat{e}_{20}^\dagger, \tag{A7}$$

$$\hat{p}_{20} = \tfrac{5}{4}\hat{e}_{20} - \tfrac{3}{4}\hat{e}_{10}^\dagger. \tag{A8}$$

The $\hat{p}_{i0}$ modes form a two-mode squeezed state. To retrieve $\hat{e}_{10}$ and $\hat{e}_{20}$, we perform a final two-mode squeezing operation on $\hat{p}_{i0}$, with squeezing parameter $t = \operatorname{arccosh}(\frac{5}{4})$, which yields

$$\cosh(t)\hat{p}_{10} + \sinh(t)\hat{p}_{20}'^\dagger = \hat{e}_{10}, \tag{A9}$$

$$\cosh(t)\hat{p}_{20} + \sinh(t)\hat{p}_{10}^\dagger = \hat{e}_{20}. \tag{A10}$$

This confirms that the teleportation protocol is fully unitary. The additional squeezing transformation is required due to the beam-splitter interaction at Bob's output port. Since some of the classical channel mode $\hat{c}_0$ is contained in the teleported mode $\hat{j}_0'$, retrieving $\hat{e}_{10}$ and $\hat{e}_{20}$ is more complicated than disentangling them via the successive inverse squeezing transformations. The three operations above can be combined into a single, inverse two-mode squeezing operation with squeezing parameter k, defined as

$$k = \ln[\cosh(t - r - s) - \sinh(t - r - s)] \tag{A11}$$

so that

$$\cosh(k)\hat{a}_0' - \sinh(k)\hat{c}_0'^\dagger = \hat{e}_{10}, \tag{A12}$$

$$\cosh(k)\hat{c}_0' - \sinh(k)\hat{a}_0'^\dagger = \hat{e}_{20}. \tag{A13}$$

As already discussed in Sec. III C, the orthogonal mode $\hat{j}_\perp$ appears in the reflected mode $\hat{c}_\perp''$.

2. Time-delayed temporal-mode telemirror

We can perform a similar analysis to retrieve the reflected mode from the temporal-mode telemirror. For simplicity, we study the scenario presented in Sec. V B, where the symmetric superposition of the input temporal modes was transmitted to Bob. Of course, this generalizes to arbitrary mode selection, shown in Appendix C 2. The operations enacted on the output modes are shown in Fig. 14. First, the output modes on the

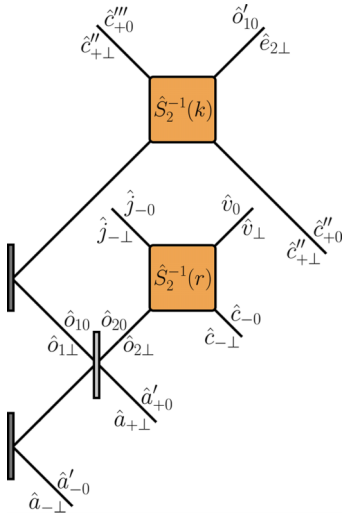

FIG. 14. Circuit diagram for the operations used to retrieve the input vacua for the temporal-mode time-delayed telemirror. We have utilized the label $\hat{j}_{-0} = (\hat{j}_{10} - \hat{j}_{20})/\sqrt{2}$ to denote the antisymmetric superposition of $\hat{j}_{i0}$.

reflected side of the telemirror are given by

$$\hat{a}_{-0} = \frac{\cosh(r)}{\sqrt{2}}(\hat{a}_0 + \hat{v}_0) + \sinh(r)\hat{j}^\dagger_{10}, \tag{A14}$$

$$\hat{a}_{+0} = \frac{\cosh(r)}{\sqrt{2}}(\hat{a}_0 - \hat{v}_0) + \sinh(r)\hat{j}^\dagger_{20}, \tag{A15}$$

$$\hat{c}_{-0} = \frac{\cosh(r)}{\sqrt{2}}(\hat{j}_{10} - \hat{j}_{20}) + \sinh(r)\hat{v}^\dagger_0, \tag{A16}$$

$$\begin{aligned}\hat{c}''_{+0} = &\left(\frac{\cosh(r)}{\sqrt{2}} - \frac{1}{2\sqrt{2}\cosh(r)}\right)(\hat{j}_{10} + \hat{j}_{20}) \\ &+ \frac{1}{2\cosh(r)}\left(\sqrt{1 - \frac{1}{2\cosh^2(r)}} - 1\right)\hat{u}_0 \\ &+ \frac{1}{2\cosh(r)}\left(\sqrt{1 - \frac{1}{2\cosh^2(r)}} + 1\right)\hat{b}_0 \\ &+ \left(\sinh(r) - \frac{\tanh(r)}{\cosh(r)}\right)\hat{a}^\dagger_0.\end{aligned} \tag{A17}$$

Mixing the $\hat{a}_{\pm 0}$ modes at a balanced beam splitter yields

$$\begin{aligned}\hat{o}_{10} &= \frac{1}{\sqrt{2}}(\hat{a}'_{+0} + \hat{a}'_{-0}) \\ &= \cosh(r)\hat{a}_0 + \frac{\sinh(r)}{\sqrt{2}}(\hat{j}^\dagger_{10} + \hat{j}^\dagger_{20}),\end{aligned} \tag{A18}$$

$$\begin{aligned}\hat{o}_{20} &= \frac{1}{\sqrt{2}}(\hat{a}'_{+0} - \hat{a}'_{-0}) \\ &= \cosh(r)\hat{v}_0 + \frac{\sinh(r)}{\sqrt{2}}(\hat{j}^\dagger_{10} - \hat{j}^\dagger_{20}).\end{aligned} \tag{A19}$$

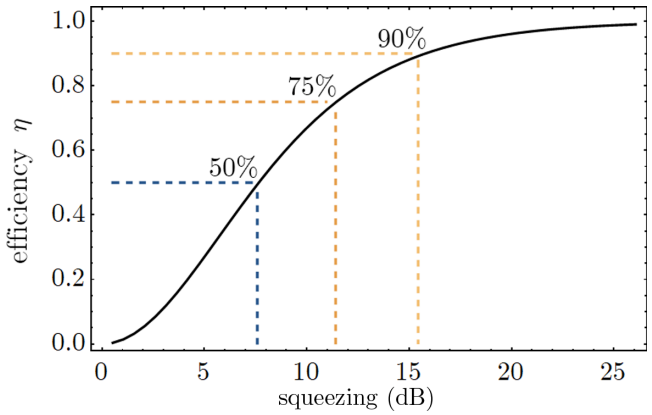

FIG. 15. Efficiency of the telefilter as a function of squeezing in decibels. The conversion between the squeezing parameter s into decibel units is given by 1 dB $= -10\log_{10}(e^{-2s})$.

Mixing $\hat{c}_{-0}$ and $\hat{o}_{20}$ at an inverse squeezer with squeezing coefficient r yields

$$\cosh(r)\hat{o}_{20} - \sinh(r)\hat{c}^\dagger_{-0} = \hat{v}_0, \tag{A20}$$

$$\cosh(r)\hat{c}_{-0} - \sinh(r)\hat{o}^\dagger_{20} = \frac{1}{\sqrt{2}}(\hat{j}_{10} - \hat{j}_{20}). \tag{A21}$$

(Note that in Fig. 14 we have utilized the labels $\hat{j}_{-0}$ and $\hat{j}_{-\perp}$ to denote the antisymmetric superposition of the input temporal modes in 0 and $\perp$, respectively.) To retrieve the input vacua $\hat{e}_{i0}$ used to generate the EPR resource, one needs to apply the series of operations shown for the atemporal representation of the protocol, which can be reduced to the action of a single unitary $\hat{S}_2(k)$ (see Appendix A). The operations are applied to the mode pair $\hat{o}_{10}$ and $\hat{c}''_{+0}$ as shown in Fig. 14. In the limit of infinite squeezing, we are able to retrieve all the leftover modes used to perform the teleportation:

$$\lim_{r\to\infty} \hat{c}'''_{+0} = \hat{e}_{10}, \tag{A22}$$

$$\lim_{r\to\infty} \hat{c}''_{+\perp} = \frac{1}{\sqrt{2}}(\hat{j}_{1\perp} + \hat{j}_{2\perp}) = \hat{j}_{+\perp}, \tag{A23}$$

$$\lim_{r\to\infty} \hat{o}'_{10} = \hat{e}_{20}. \tag{A24}$$

We see that all the orthogonal modes, i.e., $\hat{j}_{\pm\perp}$ and $\hat{j}_{-0}$, are reflected, while only $\hat{j}_{+0}$ is transmitted.

APPENDIX B: TELEFILTERS AND TELEMIRRORS WITH IMPERFECT EFFICIENCY

1. Practical efficiency of the telefilter with finite squeezing

From Eq. (35), the output mode in the atemporal representation of the telefilter with finite squeezing is given by

$$\hat{j}'''_0 = \tanh(s)\hat{j}_0 + \frac{\hat{e}_{20}}{\cosh(s)}. \tag{B1}$$

The efficiency η of the telefilter in transmitting $\hat{j}_0$ is thus given by $\tanh^2(s)$. A plot of η as a function of squeezing (in units of decibels) is shown in Fig. 15. State-of-the-art techniques in noise suppression have achieved experimental squeezing

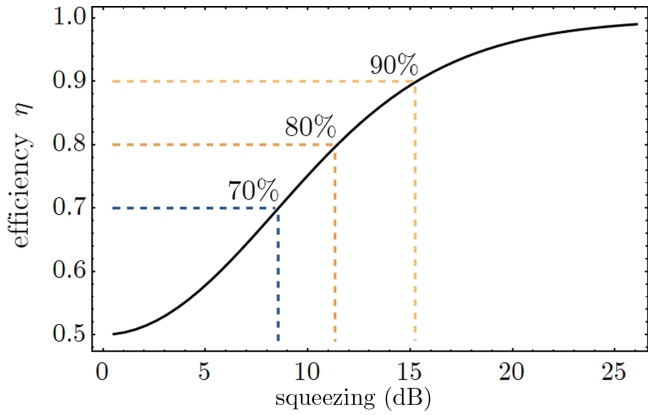

FIG. 16. Efficiency of the telemirror as a function of squeezing in decibels. The telemirror operates comparably to the telefilter.

values of ∼15 dB, which accords with ∼90% efficiency in our protocol [59].

2. All-optical telemirror with finite squeezing

In Sec. III B we presented a calculation for the atemporal representation of the mode-selective telefilter with finite squeezing. For completeness, we present here the input-output relations for the atemporal representation of the telemirror with finite squeezing. The classical channel is generated via a two-mode squeezer which couples the input mode $\hat{j}_0$ with the entanglement resource mode $\hat{a}_0$ with the gain of the channel controlled by the squeezing parameter s, that is,

$$\hat{c}_0 = \cosh(s)\hat{j}_0 + \sinh(s)\hat{a}_0^\dagger, \tag{B2}$$

$$\hat{a}_0' = \cosh(s)\hat{a}_0 + \sinh(s)\hat{j}_0^\dagger. \tag{B3}$$

Bob mixes $\hat{c}_0$ and $\hat{b}_0$ on a beam splitter with transmission coefficient

$$\eta = \frac{2\cosh^2(s)}{3+\cosh(2s)} \tag{B4}$$

so that

$$\hat{c}_0' = \sqrt{\eta}\hat{b}_0 - \sqrt{1-\eta}\hat{c}_0, \tag{B5}$$

$$\begin{aligned}\hat{j}_0' &= \sqrt{\eta}\hat{c}_0 - \sqrt{1-\eta}\hat{b}_0 \\ &= \frac{\sqrt{2}}{\sqrt{3+\cosh(2s)}}[\cosh(s)\hat{j}_0 - \hat{e}_{20}].\end{aligned} \tag{B6}$$

In Fig. 16 we have plotted the transmission coefficient η for the telemirror as a function of the squeezing in units of decibels. We see clearly that for finite squeezing levels, the output mode transmit $\hat{j}_0$ with some imperfect efficiency. In the limit of perfect squeezing, one retrieves the result for the all-optical telemirror in Sec. III C. We can also calculate the reflected modes. To do this, we perform two successive inverse squeezing operations on the reflected modes $\hat{a}_0'$ and $\hat{c}_0'$ with squeezing parameter s, yielding

$$\hat{q}_{10} = \cosh(s)\hat{a}_0' - \sinh(s)\hat{c}_0'^\dagger, \tag{B7}$$

$$\hat{q}_{20} = \cosh(s)\hat{c}_0' - \sinh(s)\hat{a}_0'^\dagger, \tag{B8}$$

$$\hat{p}_{10} = \cosh(s)\hat{q}_{10} - \sinh(s)\hat{q}_{20}^\dagger, \tag{B9}$$

$$\hat{p}_{20} = \cosh(s)\hat{q}_{20} - \sinh(s)\hat{q}_{10}^\dagger. \tag{B10}$$

A final squeezing operation with the squeezing parameter set to $\operatorname{arccosh}(\frac{5}{4})$ retrieves the vacuum modes $\hat{e}_{i0}$ in the limit of infinite squeezing. For finite squeezing, $\hat{j}_0$ appears on one of the reflected modes, complementing the part of the mode which is transmitted; obviously, this vanishes as $s \to \infty$.

3. Time-delayed temporal-mode telefilter with finite squeezing

Here we consider the temporal-mode telefilter (with two input temporal modes) with finite squeezing. This can be straightforwardly generalized to an N-mode input. The equivalent calculation for the temporal-mode telemirror is tedious but follows analogously. First, we choose the effective gain of the classical channel to be $\zeta = \tanh(s)/2\sqrt{2}|\beta|$ so that the total measurement operator is given by

$$\hat{M} = \frac{\tanh(s)}{2\sqrt{2}}(\sqrt{2}\hat{j}_{10} + \sqrt{2}\hat{j}_{20} + 2\hat{a}_0^\dagger). \tag{B11}$$

As before, we displace the output temporal components at Bob's side of the telemirror, yielding the results

$$\begin{aligned}\hat{j}_{10}' &= \frac{1}{2}(\hat{j}_{10} + \hat{j}_{20})\tanh(s) + \frac{1}{\sqrt{2}}\hat{u}_0 \\ &\quad + \frac{\tanh(s)\sinh(s) - \cosh(s)}{\sqrt{2}}\hat{e}_{20},\end{aligned} \tag{B12}$$

$$\begin{aligned}\hat{j}_{20}' &= -\frac{\tanh(s)}{2}(\hat{j}_{10} + \hat{j}_{20}) + \frac{1}{\sqrt{2}}\hat{u}_0 \\ &\quad + \frac{\cosh(s) - \tanh(s)\sinh(s)}{\sqrt{2}}\hat{e}_{20}.\end{aligned} \tag{B13}$$

For clarity, it is instructive to mix $\hat{j}_{10}'$ and $\hat{j}_{20}'$ on a balanced beam splitter, yielding

$$\hat{o}_{10}^{(l)} = \frac{1}{\sqrt{2}}(\hat{j}_{10}' + \hat{j}_{20}') \tag{B14}$$

$$= \frac{\tanh(s)}{\sqrt{2}}(\hat{j}_{10} + \hat{j}_{20}) - \frac{\hat{e}_{20}}{\cosh(s)}, \tag{B15}$$

$$\hat{o}_{10}^{(r)} = \frac{1}{\sqrt{2}}(\hat{j}_{10}' - \hat{j}_{20}') = \hat{u}_0. \tag{B16}$$

In this case, we see that the symmetric superposition of $\hat{j}_{10}$ and $\hat{j}_{20}$ has been teleported to Bob's output, with efficiency $\tanh(s)$ dictated by the amount of squeezing used to generate the entanglement-resource modes $\hat{a}_0$ and $\hat{b}_0$. In the limit of perfect entanglement, we simply obtain the result shown in Eqs. (65) and (66). To generalize this result to an N-mode input, one must appropriately choose the effective gain ξ of the classical channel so that the channel between Alice and Bob is the identity [see, for example, the prefactor of Eq. (B11)].

APPENDIX C: SELECTING AN ARBITRARY SUPERPOSITION MODE USING THE TEMPORAL-MODE TELEFILTER AND TELEMIRROR

In the main text, we demonstrated simple examples where the telefilter and telemirror transmitted a particular superposition of the input temporal modes and filtering or reflecting all others. Here we generalize those result to show that any arbitrary mode can be selected by these devices, with the orthogonal modes filtered or reflected. We present the general calculations in the same order in which they appear in the main text (corresponding to Secs. V A, V B, VI B, and VI C respectively).

1. Time-delayed temporal-mode telefilter

To select an arbitrary mode with the time-delayed temporal-mode telefilter, we require some additional degrees of freedom in our setup. Previously, the measurement operators were constructed from the $\hat{X}$ and $\hat{P}$ quadratures from the output modes at the dual homodyne measurement. In full generality, we can construct these measurement operators using quadrature operators at an arbitrary phase with a $\pi/2$ phase shift between them, that is,

$$\hat{X}_{a_{-0}}(\phi_1) = \hat{a}'_{-0}e^{-i\phi_1} + \hat{a}'^{\dagger}_{-0}e^{i\phi_1}, \tag{C1}$$

$$\hat{X}_{j_{10'}}(\phi'_1) = \hat{j}'_{10}e^{-i\phi'_1} + \hat{j}'^{\dagger}_{10}e^{i\phi'_1}, \tag{C2}$$

$$\hat{X}_{a_{+0}}(\phi_2) = \hat{a}_{+0}e^{-i\phi_2} + \hat{a}_{+0}e^{i\phi_2}, \tag{C3}$$

$$\hat{X}_{j'_{20}}(\phi'_2) = \hat{j}'_{20}e^{-i\phi'_2} + \hat{j}'^{\dagger}_{20}e^{i\phi'_2}, \tag{C4}$$

where $\phi'_i = \phi_i + \pi/2$. The measurement operators are now given by

$$\hat{M}_1 = \sqrt{2}|\beta|(e^{-i\phi_1}\hat{j}_{10} - i\sqrt{1-\alpha}e^{i(\phi+\phi_1)}\hat{a}^{\dagger}_0 - \sqrt{\alpha}e^{i\phi_1}\hat{v}^{\dagger}_0), \tag{C5}$$

$$\hat{M}_2 = \sqrt{2}|\beta|(e^{-i\phi_2}\hat{j}_{20} - \sqrt{\alpha}e^{i\phi_2}\hat{a}^{\dagger}_0 - i\sqrt{1-\alpha}e^{-i(\phi-\phi_2)}\hat{v}^{\dagger}_0). \tag{C6}$$

We add these together in the usual way,

$$\hat{M} = \zeta_1(\phi_1,\alpha)\hat{M}_1 + \zeta_2(\phi_2,\alpha)\hat{M}_2, \tag{C7}$$

with the following choices for the weighting of the individual measurements:

$$\zeta_1(\phi_1,\alpha) = \frac{1-\alpha}{\sqrt{2}\lambda_1}e^{-i\phi_1}, \tag{C8}$$

$$\zeta_2(\phi_2,\alpha) = \frac{\sqrt{\alpha(1-\alpha)}}{\sqrt{2}\lambda_1}e^{-i\phi_2}. \tag{C9}$$

We displace Bob's entanglement resource modes using the total measurement operator

$$\hat{j}'_{10} = \hat{b}_{-0} + \lambda_1(\alpha)\hat{M}, \tag{C10}$$

$$\hat{j}'_{20} = \hat{b}_{+0} + \lambda_2(\alpha)\hat{M}, \tag{C11}$$

with the relationship

$$\lambda_2(\alpha) = \frac{\lambda_1\sqrt{\alpha}}{\sqrt{1-\alpha}}. \tag{C12}$$

Mixing the output modes on a passive beam splitter yields

$$\begin{aligned}\hat{o}^{(l)}_{10} &= \sqrt{\alpha}\hat{j}'_{20} + \sqrt{1-\alpha}\hat{j}'_{10}\\ &= e^{-2i\phi_1}\sqrt{1-\alpha}\hat{j}_{10} + e^{-2i\phi_2}\sqrt{\alpha}\hat{j}_{20}\\ &\quad + (\hat{b}_0 - \hat{a}^{\dagger}_0),\end{aligned} \tag{C13}$$

$$\hat{o}^{(r)}_{10} = \sqrt{\alpha}\hat{j}'_{10} - \sqrt{1-\alpha}\hat{j}'_{20} = \hat{u}_0. \tag{C14}$$

By tuning the quadrature phases ϕ_i and the beam-splitter transmission coefficient α, Alice can select any arbitrary mode to transmit to Bob in $\hat{o}^{(l)}_{10}$, while the other mode contains vacuum.

2. Time-delayed temporal-mode telemirror

An analogous calculation can be performed for the time-delayed temporal-mode telemirror. The extra degrees of freedom we introduce are phase shifts on the classical channel modes, namely,

$$\hat{U}^{\dagger}(\phi_j)\hat{j}\hat{U}(\phi_j) = \hat{j}e^{i\phi_j}, \tag{C15}$$

where $\hat{j} = \hat{c}_{i0}, \hat{a}'_{\pm 0}$. To obtain the desired output, let us impose the following constraints on the beam-splitter phases:

$$\begin{aligned}\theta_- &= \phi + \theta_+ + \frac{\pi}{2}, \quad \theta_+ = \phi_{c_{20}} + \frac{\pi}{2},\\ \phi_{c_{10}} &= -\phi + \frac{\pi}{2}, \quad \phi_{c_0} = \phi + \phi_{c_{10}} - \phi_{c_{20}}.\end{aligned} \tag{C16}$$

Another set of constraints could have been chosen, since the choice above is not unique. This yields the output modes

$$\begin{aligned}\hat{j}'_{10} &= (1-\alpha)e^{-2i\phi}\hat{j}_{10} + ie^{-i\phi}\sqrt{\alpha(1-\alpha)}\hat{j}_{20}\\ &\quad - ie^{-i\phi}\sqrt{1-\alpha}(\hat{b}_0 - \hat{a}^{\dagger}_0) + \sqrt{\alpha}\hat{u}_0,\end{aligned} \tag{C17}$$

$$\begin{aligned}\hat{j}'_{20} &= ie^{-i\phi}\sqrt{\alpha(1-\alpha)}\hat{j}_{10} - \alpha\hat{j}_{20} + \sqrt{\alpha}(\hat{b}_0 - \hat{a}^{\dagger}_0)\\ &\quad - ie^{i\phi}\sqrt{1-\alpha}\hat{u}_0.\end{aligned} \tag{C18}$$

These output modes are mixed at a final passive beam splitter,

$$\hat{o}^{(l)}_{10} = \sqrt{\alpha}\hat{j}'_{20} - ie^{-i\chi}\sqrt{1-\alpha}\hat{j}'_{10}, \tag{C19}$$

$$\hat{o}^{(r)}_{10} = \sqrt{\alpha}\hat{j}'_{10} - ie^{i\chi}\sqrt{1-\alpha}\hat{j}'_{20}. \tag{C20}$$

By taking $\chi = -\phi + \pi$ we obtain the desired result,

$$\hat{o}^{(l)}_{10} = ie^{-i\phi}\sqrt{1-\alpha}\hat{j}_{10} - \sqrt{\alpha}\hat{j}_{20} + (\hat{b}_0 - \hat{a}^{\dagger}_0), \tag{C21}$$

$$\hat{o}^{(r)}_{10} = \hat{u}_0. \tag{C22}$$

Thus, Alice may select any arbitrary mode to be transmitted to Bob. For the reflected modes, we first mix the outputs from the two-mode squeezers at a passive beam splitter:

$$\hat{o}_{10} = \sqrt{\mu}\hat{a}'_{-0} - ie^{-i\phi_{a_{+0}}}\sqrt{1-\mu}\hat{a}'_{+0}, \tag{C23}$$

$$\hat{o}_{20} = \sqrt{\mu}\hat{a}'_{+0} - ie^{i\phi_{a_{+0}}}\sqrt{1-\mu}\hat{a}'_{-0}. \tag{C24}$$

We then inverse squeeze $\hat{o}_{20}$ with the output from the mixing of the classical channel modes $\hat{c}_{-0}$:

$$\hat{r}_{10} = \cosh(r)\hat{o}_{20} - \sinh(r)\hat{c}^{\dagger}_{-0}, \tag{C25}$$

$$\hat{r}_{20} = \cosh(r)\hat{c}_{-0} - \sinh(r)\hat{o}^{\dagger}_{20}. \tag{C26}$$

Like before, we can make the following choices for the beamsplitter phases:

$$\phi_{c_{10}} = -\phi + \frac{\pi}{2}, \quad \phi_{a_{+0}} = \phi - \phi_{a_{-0}}. \tag{C27}$$

This yields the output modes

$$\hat{r}_{10} = -ie^{i\phi}\hat{v}_0, \tag{C28}$$

$$\hat{r}_{20} = ie^{-i\phi}\sqrt{\alpha}\hat{j}_{10} + \sqrt{1-\alpha}\hat{j}_{20}. \tag{C29}$$

The mode $\hat{r}_{20}$ is orthogonal to $\hat{o}_{10}^{(l)}$, giving the desired mode-selective property of the result.

3. No-delay temporal-mode telefilter

For completeness, we show how the no-delay telefilter and telemirror can be generalized to partially select an arbitrary mode of interest. As before, we define our quadrature operators with the generic phase ϕ_i. We construct the measurement operators

$$\hat{M}_1 = \hat{X}_{a_{-0}}(\phi_1) + i\hat{X}_{j'_{10}}(\phi''_1), \tag{C30}$$

$$\hat{M}_2 = \hat{X}_{a_{+0}}(\phi_2) + i\hat{X}_{j'_{20}}(\phi''_2), \tag{C31}$$

which are used to displace the entanglement resource modes,

$$\hat{j}'_{10} = \hat{b}_{-0} + \lambda_1(\phi_1)\hat{M}_1, \tag{C32}$$

$$\hat{j}'_{20} = \hat{b}_{+0} + \lambda_2(\phi_2)\hat{M}_2. \tag{C33}$$

We obtain the output modes

$$\hat{j}'_{10} = e^{-2i\phi_1}\hat{j}_{10} + \sqrt{1-\alpha}(\hat{b}_0 - \hat{a}_0^\dagger) + \sqrt{\alpha}(\hat{u}_0 - \hat{v}_0^\dagger), \tag{C34}$$

$$\hat{j}'_{20} = e^{-2i\phi_2}\hat{j}_{20} + \sqrt{\alpha}(\hat{b}_0 - \hat{a}_0^\dagger), \tag{C35}$$

where we have retained the nomenclature for the quadrature phases in Appendix C 1. Mixing these back on a passive beam splitter in the usual way yields

$$\hat{o}_{10}^{(l)} = e^{-2i\phi_1}\sqrt{1-\alpha}\hat{j}_{10} + e^{-2i\phi_2}\sqrt{\alpha}\hat{j}_{20} + (\hat{b}_0 - \hat{a}_0^\dagger), \tag{C36}$$

$$\hat{o}_{10}^{(r)} = e^{-2i\phi_1}\sqrt{\alpha}\hat{j}_{10} - e^{-2i\phi_2}\sqrt{1-\alpha}\hat{j}_{20} + (\hat{u}_0 - \hat{v}_0^\dagger). \tag{C37}$$

Now the mode of interest with phases ϕ_i and transmission coefficient α appears in $\hat{o}_{10}^{(l)}$ with its complement in the other transmitted mode $\hat{o}_{10}^{(r)}$.

4. No-delay temporal-mode telemirror

For the no-delay temporal-mode telemirror, Alice could generate the squeezing classical channels with squeezing phases θ_{s_i},

$$\hat{c}_{10} = \cosh(r)\hat{j}_{10} - e^{i\phi_{c_{10}}}\sinh(r)\hat{a}_{-0}^\dagger, \tag{C38}$$

$$\hat{c}_{20} = \cosh(r)\hat{j}_{20} - e^{i\phi_{c_{20}}}\sinh(r)\hat{a}_{+0}^\dagger. \tag{C39}$$

We perform the usual displacement of Bob's individual entanglement resource modes using these channel modes:

$$\hat{j}'_{10} = \sqrt{\eta_-}\hat{b}_{-0} - ie^{i\theta_-}\sqrt{1-\eta_-}\hat{c}_{10}, \tag{C40}$$

$$\hat{j}'_{20} = \sqrt{\eta_+}\hat{b}_{+0} - ie^{i\theta_+}\sqrt{1-\eta_+}\hat{c}_{20}. \tag{C41}$$

As before, we can make simplifications by choosing the beamsplitter phases, knowing the desired outcome of the partially mode-selective mirror. For example, taking

$$\phi = -\pi/2, \tag{C42}$$

$$\phi_{c_{10}} = \pi/2 - \theta_-, \tag{C43}$$

$$\phi_{c_{20}} = \theta_- - \theta_+ + \phi_{c_{10}} \tag{C44}$$

yields the outputs (in the limit of high gain $r \to \infty$)

$$\hat{j}'_{10} = -ie^{i\theta_-}\hat{j}_{10} + \sqrt{1-\alpha}(\hat{b}_0 - \hat{a}_0^\dagger) + \sqrt{\alpha}(\hat{u}_{10} - \hat{v}_{10}^\dagger), \tag{C45}$$

$$\hat{j}'_{20} = -ie^{i\theta_+}\hat{j}_{20} + \sqrt{\alpha}(\hat{b}_0 - \hat{a}_0^\dagger) - \sqrt{1-\alpha}(\hat{u}_{10} - \hat{v}_{10}^\dagger). \tag{C46}$$

Mixing these on a final beam splitter yields

$$\hat{o}_{10}^{(l)} = -ie^{i\theta_-}\sqrt{1-\alpha}\hat{j}_{10} - ie^{i\theta_+}\sqrt{\alpha}\hat{j}_{20} + (\hat{b}_0 - \hat{a}_0^\dagger), \tag{C47}$$

$$\hat{o}_{10}^{(r)} = -ie^{i\theta_-}\sqrt{\alpha}\hat{j}_{10} + ie^{i\theta_+}\sqrt{1-\alpha}\hat{j}_{20} + (\hat{u}_{10} - \hat{v}_{10}^\dagger). \tag{C48}$$

Thus, Alice can select an arbitrary mode to be mode discriminated, with the orthogonal superposition transmitted along with noise. We are less interested in the reflected modes in this case, since the device does not isolate the mode of interest on either the transmitted or reflected sides.

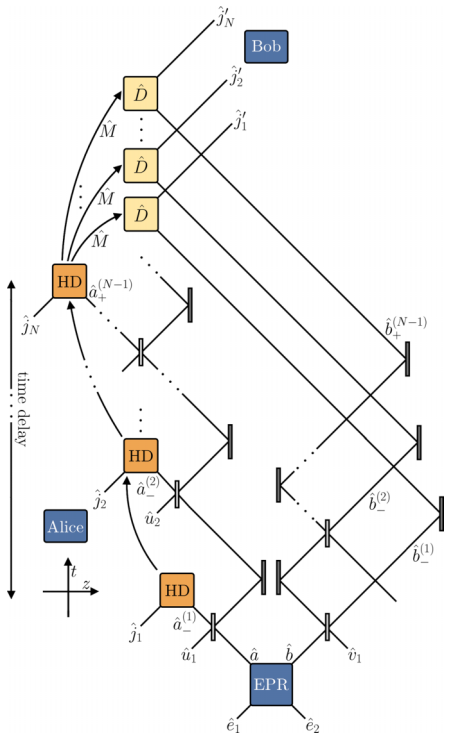

FIG. 17. Circuit diagram for the N-mode temporal-mode time-delayed telefilter.

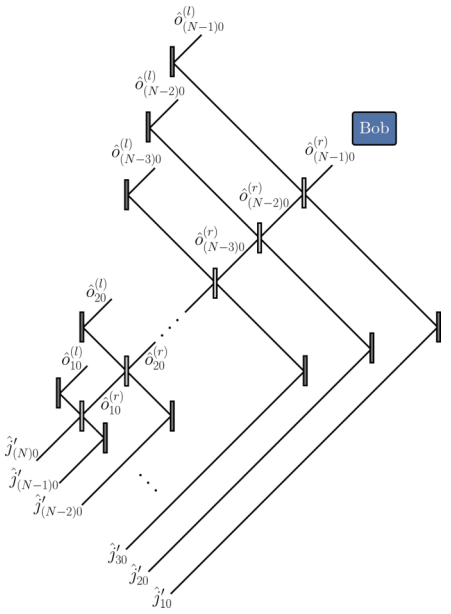

FIG. 18. Circuit for the recombination of the output modes used to retrieve the mode of interest.

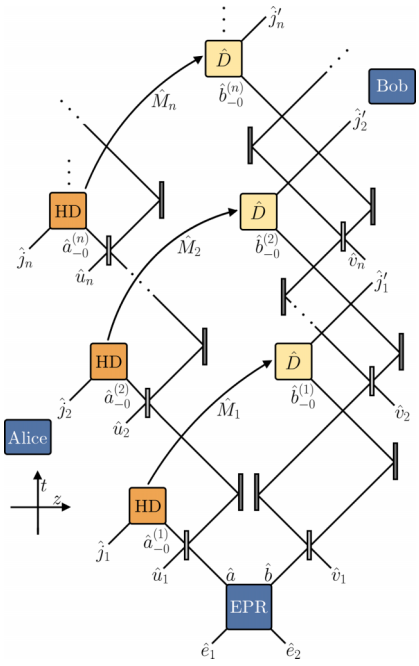

FIG. 19. Circuit diagram for the N-mode temporal-mode telefilter with no time-delay.

APPENDIX D: N-MODE GENERALIZATION

We now generalize the temporal-mode telefilter protocols studied in the main text to an input of N temporal modes. In the large-N limit, the input approximates an input wave packet decomposed into a large number of orthogonal modes. Although the telefilter and telemirror protocols possess a direct mapping between one another, the calculations for the telefilter are much simpler, particularly for the time-delayed case. For brevity, we only present the N-mode extension of the telefilter, in both the time-delayed and no-delay cases.

1. N-mode temporal-mode time-delayed telefilter

We have the circuit shown in Fig. 17. This is the N-mode extension of the temporal-mode time-delayed telefilter discussed in Sec. V A. The N temporal-mode inputs are mixed with N respective local oscillators, which are likewise mode matched with the entanglement resource modes $\hat{a}_{-0}^{(n)}\cdots\hat{a}_{+0}^{(N-1)}$. These entanglement resource modes are distributed among the N temporal modes via passive beam splitters with transmission coefficient α_i and phase ϕ_i as follows:

$$
\begin{aligned}
\hat{a}_{-0}^{(1)} &= \sqrt{\alpha_1}\hat{v}_{10} - ie^{-i\phi_1}\hat{a}_0, & \hat{b}_{-0}^{(1)} &= \sqrt{\alpha_1}\hat{u}_{10} - ie^{-i\phi_1}\hat{b}_0,\\
\hat{a}_{+0}^{(1)} &= \sqrt{\alpha_1}\hat{a}_0 - ie^{i\phi_1}\sqrt{1-\alpha_1}\hat{v}_{10}, & \hat{b}_{+0}^{(1)} &= \sqrt{\alpha_1}\hat{b}_0 - ie^{i\phi_1}\sqrt{1-\alpha_1}\hat{u}_0,\\
\hat{a}_{-0}^{(2)} &= \sqrt{\alpha_2}\hat{v}_{20} - ie^{-i\phi_2}\hat{a}_{+0}^{(1)}, & \hat{b}_{-0}^{(2)} &= \sqrt{\alpha_2}\hat{u}_{20} - ie^{-i\phi_2}\hat{b}_{+0}^{(1)},\\
\hat{a}_{+0}^{(2)} &= \sqrt{\alpha_2}\hat{a}_{+0}^{(1)} - ie^{i\phi_2}\sqrt{1-\alpha_2}\hat{v}_{20}, & \hat{b}_{+0}^{(2)} &= \sqrt{\alpha_2}\hat{b}_{+0}^{(1)} - ie^{i\phi_2}\sqrt{1-\alpha_2}\hat{u}_{20},\\
&\vdots & &\vdots\\
\hat{a}_{-0}^{(n)} &= \sqrt{\alpha_n}\hat{v}_{n0} - ie^{-i\phi_n}\sqrt{1-\alpha_n}\hat{a}_{+0}^{(n-1)}, & \hat{b}_{-0}^{(n)} &= \sqrt{\alpha_n}\hat{u}_{n0} - ie^{-i\phi_n}\sqrt{1-\alpha_n}\hat{b}_{+0}^{(n-1)},\\
\hat{a}_{+0}^{(n)} &= \sqrt{\alpha_n}\hat{a}_{+0}^{(n-1)} - ie^{i\phi_n}\sqrt{1-\alpha_n}\hat{v}_{n0}, & \hat{b}_{+0}^{(n)} &= \sqrt{\alpha_n}\hat{b}_{+0}^{(n-1)} - ie^{i\phi_n}\sqrt{1-\alpha_n}\hat{u}_{n0},\\
&\vdots & &\vdots\\
\hat{a}_{-0}^{(N-1)} &= \sqrt{\alpha_{N-1}}\hat{v}_{(N-1)0} - ie^{-i\phi_{N-1}}\sqrt{1-\alpha_{N-1}}\hat{a}_{+0}^{(N-2)}, & \hat{b}_{-0}^{(N-1)} &= \sqrt{\alpha_{N-1}}\hat{u}_{(N-1)0} - ie^{-i\phi_{N-1}}\sqrt{1-\alpha_{N-1}}\hat{b}_{+0}^{(N-2)},\\
\hat{a}_{+0}^{(N-1)} &= \sqrt{\alpha_{N-1}}\hat{a}_{+0}^{(N-2)} - ie^{i\phi_{N-1}}\sqrt{1-\alpha_{N-1}}\hat{v}_{(N-1)0}, & \hat{b}_{+0}^{(N-1)} &= \sqrt{\alpha_{N-1}}\hat{b}_{+0}^{(N-2)} - ie^{i\phi_{N-1}}\sqrt{1-\alpha_{N-1}}\hat{u}_{(N-1)0}.
\end{aligned}
$$

Some fraction of the original entanglement, $\hat{a}_0$ and $\hat{b}_0$, is distributed to each temporal mode and used to obtain the measurement result. At this point, let us specialize to $\phi_i = -\pi/2$ for the beam-splitter phases for simplicity. Of course, one can choose this arbitrarily to select a different mode; this then requires a specifically tuned recombination of the output modes on Bob's

transmitted side. Here we simply present an example which illustrates the generic process for selecting a mode to be transmitted from Alice to Bob. For further simplification, we will take the measurement results to be

$$\hat{M}_1 = |\beta|\big(\hat{X}_{a^{(1)}_{-0}} + i\hat{P}_{j'_{20}}\big) = \sqrt{2}|\beta|(\hat{j}_{10} - \sqrt{1-\alpha}\hat{a}^\dagger_0 - \sqrt{\alpha_1}\hat{v}^\dagger_{10}), \tag{D1}$$

$$\hat{M}_2 = |\beta|\big(\hat{X}_{a^{(2)\prime}_{-0}} + i\hat{P}_{j'_{20}}\big) = \sqrt{2}|\beta|(\hat{j}_{20} - \sqrt{\alpha(1-\alpha_2)}\hat{a}^\dagger_0 + \sqrt{(1-\alpha_1)(1-\alpha_2)}\hat{v}^\dagger_{10} - \sqrt{\alpha_2}\hat{v}^\dagger_{20}), \tag{D2}$$

$$\vdots$$

$$\begin{aligned}\hat{M}_n = |\beta|\big(\hat{X}_{a^{(n)\prime}_{-0}} + i\hat{P}_{j'_{(n)0}}\big) = \sqrt{2}|\beta|(&\hat{j}_{n0} - \sqrt{\alpha_1\alpha_2\cdots(1-\alpha_n)}\hat{a}^\dagger_0 + \sqrt{(1-\alpha_1)\alpha_2\cdots\alpha_{n-1}(1-\alpha_n)}\hat{v}^\dagger_{10}\\ &+ \sqrt{(1-\alpha_2)\alpha_3\cdots\alpha_{n-1}(1-\alpha_n)}\hat{v}^\dagger_{20} + \cdots + \sqrt{(1-\alpha_{n-1})(1-\alpha_n)}\hat{v}^\dagger_{(n-1)0} - \sqrt{\alpha_n}\hat{v}^\dagger_{(n)0}),\end{aligned} \tag{D3}$$

$$\vdots$$

$$\begin{aligned}\hat{M}_N = |\beta|\big(\hat{X}_{a^{(N-1)\prime}_{+0}} + i\hat{P}_{j'_{(N)0}}\big) = \sqrt{2}|\beta|(&\hat{j}_{(N)0} - \sqrt{\alpha_1\cdots\alpha_{N-1}}\hat{a}^\dagger_0 + \sqrt{(1-\alpha_1)\alpha_2\cdots\alpha_{N-1}}\hat{v}^\dagger_{10}\\ &+ \sqrt{(1-\alpha_2)\alpha_3\cdots\alpha_{N-1}}\hat{v}^\dagger_{20} + \cdots + \sqrt{1-\alpha_{N-1}}\hat{v}^\dagger_{(N-1)0}).\end{aligned} \tag{D4}$$

We add these to form a total measurement operator $\hat{M} = \sum_{i=1}^N \zeta_i \hat{M}_i$, where

$$\zeta_1 = \frac{\zeta_N\sqrt{1-\alpha_1}}{\sqrt{\alpha_1\alpha_2\cdots\alpha_{N-1}}}, \quad \zeta_2 = \frac{\zeta_N\sqrt{1-\alpha_2}}{\sqrt{\alpha_2\alpha_3\cdots\alpha_{N-1}}}, \ldots, \quad \zeta_n = \frac{\zeta_N\sqrt{1-\alpha_n}}{\sqrt{\alpha_n\alpha_{n+1}\cdots\alpha_{N-1}}}, \ldots, \quad \zeta_{N-1} = \frac{\zeta_N\sqrt{1-\alpha_{N-1}}}{\sqrt{\alpha_{N-1}}}. \tag{D5}$$

As shown in Fig. 17, one may partition the input field into a larger number of time-bin modes to obtain a better approximation to a continuous wave packet. Overall, the total time delay is the difference in the arrival times of the first and last time-bin modes. Now the total measurement operator is used to displace the N entanglement resource modes sent to Bob's side of the telefilter,

$$\hat{j}'_{10} = \hat{b}^{(1)}_{-0} + \lambda_1\hat{M}, \quad \hat{j}'_{20} = \hat{b}^{(2)}_{-0} + \lambda_2\hat{M}_2, \ldots, \quad \hat{j}_{(n)0} = \hat{b}^{(n)}_{-0} + \lambda_n\hat{M}_n, \ldots, \quad \hat{j}'_{(N)0} = \hat{b}^{(N-1)}_{+0} + \lambda_N\hat{M}_N, \tag{D6}$$

where we need to choose the effective gains in a likewise weighted fashion,

$$\lambda_1 = \frac{\sqrt{(1-\alpha_1)\alpha_1\alpha_2\cdots\alpha_{N-1}}}{|\beta|\sqrt{2}\zeta_N}, \quad \lambda_2 = \frac{\alpha_1\sqrt{(1-\alpha_2)\alpha_2\cdots\alpha_{N-1}}}{|\beta|\sqrt{2}\zeta_N}, \ldots, \quad \lambda_n = \frac{\alpha_1\alpha_2\cdots\alpha_{n-1}\sqrt{(1-\alpha_n)\alpha_n\cdots\alpha_{N-1}}}{|\beta|\sqrt{2}\zeta_N}, \tag{D7}$$

$$\lambda_N = \frac{\alpha_1\alpha_2\cdots\alpha_{N-1}\alpha_N}{|\beta|\sqrt{2}\zeta_N}. \tag{D8}$$

To retrieve the teleported mode, we mix these back together on weighted beam splitters (see Fig. 18) as

$$\begin{aligned}
\hat{o}^{(l)}_{10} &= \sqrt{\alpha_{N-1}}\hat{j}'_{(N-1)0} - \sqrt{1-\alpha_{N-1}}\hat{j}'_{(N)0}, & \hat{o}^{(r)}_{10} &= \sqrt{\alpha_{N-1}}\hat{j}'_{(N)0} + \sqrt{1-\alpha_{N-1}}\hat{j}'_{(N-1)0},\\
\hat{o}^{(l)}_{20} &= \sqrt{\alpha_{N-2}}\hat{j}'_{(N-2)0} - \sqrt{1-\alpha_{N-2}}\hat{o}^{(r)}_{10}, & \hat{o}^{(r)}_{20} &= \sqrt{\alpha_{N-2}}\hat{o}^{(r)}_{10} + \sqrt{1-\alpha_{N-2}}\hat{j}'_{(N-2)0},\\
&\vdots & &\vdots\\
\hat{o}^{(l)}_{(n)0} &= \sqrt{\alpha_{N-n}}\hat{j}'_{(N-n)0} - \sqrt{1-\alpha_{N-n}}\hat{o}^{(r)}_{(n-1)0}, & \hat{o}^{(r)}_{(n)0} &= \sqrt{\alpha_{N-n}}\hat{o}^{(r)}_{(n-1)0} + \sqrt{1-\alpha_{N-n}}\hat{j}'_{(N-n)0},\\
&\vdots & &\vdots\\
\hat{o}^{(l)}_{(N-1)0} &= \sqrt{\alpha_1}\hat{j}'_{10} - \sqrt{1-\alpha_1}\hat{o}^{(r)}_{(N-1)0}, & \hat{o}^{(r)}_{(N-1)0} &= \sqrt{\alpha_1}\hat{o}^{(r)}_{(N-1)0} + \sqrt{1-\alpha_1}\hat{j}'_{10},
\end{aligned}$$

which yields the outputs

$$\begin{aligned}
\hat{o}^{(l)}_{10} &= \hat{u}_{(N-1)0},\\
\hat{o}^{(l)}_{20} &= \hat{u}_{(N-2)0},\\
&\vdots\\
\hat{o}^{(l)}_{(N-2)0} &= \hat{u}_{20},\\
\hat{o}^{(l)}_{(N-1)0} &= \sqrt{1-\alpha}\hat{j}_{10} + \sqrt{\alpha(1-\alpha)}\hat{j}_{20} + \sqrt{\alpha_1\alpha_2(1-\alpha_3)}\hat{j}_{30}\\
&\quad + \cdots + \sqrt{\alpha_1\cdots\alpha_{N-2}(1-\alpha_{N-1})}\hat{j}_{(N-1)0} + \sqrt{\alpha_1\cdots\alpha_{N-1}}\hat{j}_{(N)0},\\
\hat{o}^{(r)}_{(N-1)0} &= \hat{u}_{10}.
\end{aligned}$$

All of the output modes except $\hat{o}^{(l)}_{(N-1)0}$ contain the vacuum modes $\hat{u}_{(n)0}$. Only $\hat{o}^{(l)}_{(N-1)0}$ contains the selected superposition of the N temporal modes (here with equal phases between the constituent modes), which is the desired action of the mode-selective telefilter.

2. *N*-mode temporal-mode no-delay telefilter

We have the circuit shown in Fig. 19. Our entanglement is split up in the same way as the time-delayed telefilter case. As before, let us specialize to $\phi_i = -\pi/2$ for the beam-splitter phases, for simplicity. We can construct the individual measurement results from the quadrature operators obtained at each homodyne measurement as follows:

$$\hat{M}_1 = |\beta|\big(\hat{X}_{j'_{10}} + i\hat{P}_{a^{(1)\prime}_{-0}}\big) = \sqrt{2}|\beta|(\hat{j}_{10} + \sqrt{1-\alpha_1}\hat{a}^\dagger_0 + \sqrt{\alpha_1}\hat{v}_{10}), \tag{D9}$$

$$\hat{M}_2 = |\beta|\big(\hat{X}_{j'_{20}} + i\hat{P}_{a^{(2)\prime}_{-0}}\big) = \sqrt{2}|\beta|[\hat{j}_{20} + \sqrt{\alpha_1(-\alpha_2)}\hat{a}^\dagger_0 - \sqrt{(1-\alpha_1)(1-\alpha_2)}\hat{v}^\dagger_{10} + \sqrt{\alpha_2}\hat{v}^\dagger_{20}], \tag{D10}$$

$$\vdots$$

$$\begin{aligned}\hat{M}_n = |\beta|\big(\hat{X}_{j'_{(n)0}} + i\hat{P}_{a^{(n)\prime}_{-0}}\big) = \sqrt{2}|\beta|[&\hat{j}_{n0} + \sqrt{\alpha_1\alpha_2\cdots\alpha_{n-1}(1-\alpha_n)}\hat{a}^\dagger_0 - \sqrt{(1-\alpha_1)\alpha_2\cdots\alpha_{n-1}(1-\alpha_n)}\hat{v}^\dagger_{10} \\ &- \sqrt{(1-\alpha_2)\alpha_3\cdots\alpha_{n-1}(1-\alpha_n)}\hat{v}^\dagger_{20} - \cdots - \sqrt{(1-\alpha_{n-1})(1-\alpha_n)}\hat{v}^\dagger_{(n-1)0} + \sqrt{\alpha_n}\hat{v}^\dagger_{(n)0}],\end{aligned} \tag{D11}$$

$$\vdots$$

$$\begin{aligned}\hat{M}_N = |\beta|\big(\hat{X}_{j'_{N0}} + i\hat{P}_{a^{(N-1)\prime}_{+0}}\big) = \sqrt{2}|\beta|[&\hat{j}_{(N)0} + \sqrt{\alpha_1\cdots\alpha_{N-1}}\hat{a}^\dagger_0 - \sqrt{(1-\alpha_1)\alpha_2\cdots\alpha_{N-1}}\hat{v}^\dagger_{10} - \sqrt{(1-\alpha_2)\alpha_3\cdots\alpha_{N-1}}\hat{v}^\dagger_{20} \\ &- \sqrt{(1-\alpha_{N-2})\alpha_{N-1}}\hat{v}^\dagger_{(N-2)0} - \sqrt{1-\alpha_{N-1}}\hat{v}^\dagger_{(N-1)0}].\end{aligned} \tag{D12}$$

We use these measurement results to displace Bob's half of the entanglement resource modes. We choose the effective gain of the displacement to be $\zeta_i = -1/\sqrt{2}|\beta|$, which yields an identity channel between Alice and Bob for each of the temporal modes:

$$\hat{j}'_{10} = -\hat{j}_{10} + \sqrt{1-\alpha_1}(\hat{b}_0 - \hat{a}^\dagger_0) + \sqrt{\alpha_1}(\hat{u}_{10} - \hat{v}^\dagger_{10}), \tag{D13}$$

$$\hat{j}'_{20} = -\hat{j}_{20} + \sqrt{\alpha_1(1-\alpha_2)}(\hat{b}_0 - \hat{a}^\dagger_0) - \sqrt{(1-\alpha_1)(1-\alpha_2)}(\hat{u}_{10} - \hat{v}^\dagger_{10}) + \sqrt{\alpha_2}(\hat{u}_{20} - \hat{v}^\dagger_{20}), \tag{D14}$$

$$\vdots$$

$$\begin{aligned}\hat{j}'_{(n)0} = -\hat{j}_{(n)0} + \sqrt{\alpha_1\alpha_2\cdots(1-\alpha_n)}(\hat{b}_0 - \hat{a}^\dagger_0) - \sqrt{(1-\alpha_1)\alpha_2\cdots\alpha_{n-1}(1-\alpha_n)}(\hat{u}_{10} - \hat{v}^\dagger_{10}) \\ - \sqrt{(1-\alpha_2)\alpha_3\cdots\alpha_{n-1}(1-\alpha_n)}(\hat{u}_{20} - \hat{v}^\dagger_{20}) - \cdots - \sqrt{(1-\alpha_{n-1})(1-\alpha_n)}(\hat{u}_{(n-1)0} - \hat{v}^\dagger_{(n-1)0}) + \sqrt{\alpha_n}(\hat{u}_{(n)0} - \hat{v}^\dagger_{(n)0}),\end{aligned} \tag{D15}$$

$$\vdots$$

$$\begin{aligned}\hat{j}'_{(N)0} = -\hat{j}_{(N)0} - \sqrt{(1-\alpha_1)\alpha_2\cdots\alpha_{N-1}}(\hat{u}_{10} - \hat{v}^\dagger_{10}) - \sqrt{(1-\alpha_2)\alpha_3\cdots\alpha_{N-1}}(\hat{u}_{20} - \hat{v}^\dagger_{20}) \\ - \cdots - \sqrt{(1-\alpha_{N-2}\alpha_{N-1}}(\hat{u}_{(N-2)0} - \hat{v}^\dagger_{(N-2)0}) - \sqrt{1-\alpha_{N-1}}(\hat{u}_{(N-1)0} - v^\dagger_{(N-1)0}).\end{aligned} \tag{D16}$$

Performing a similar recombination of the output modes on passive beam splitters (which are weighted in with respect to the initial distribution of the entanglement resource modes across different temporal modes), we finally obtain

$$\hat{o}^{(l)}_{10} = -\sqrt{\alpha_{N-1}}\hat{j}_{(N-1)0} + \sqrt{1-\alpha_{N-1}}\hat{j}_{(N)0} + \underbrace{(\hat{u}_{(N-1)0} - v^\dagger_{(N-1)0})}_{\text{noise}},$$

$$\hat{o}^{(l)}_{20} = -\sqrt{\alpha_{N-2}}\hat{j}_{(N-2)0} + \sqrt{(1-\alpha_{N-2})(1-\alpha_{N-1})}\hat{j}_{(N-1)0} + \sqrt{(1-\alpha_{N-2})\alpha_{N-1}}\hat{j}_{(N)0} + \underbrace{(\hat{u}_{(N-2)0} - \hat{v}^\dagger_{(N-2)0})}_{\text{noise}},$$

$$\vdots$$

$$\begin{aligned}\hat{o}^{(l)}_{(n)0} = &-\sqrt{\alpha_{N-n}}\hat{j}_{(N-n)0} + \sqrt{(1-\alpha_{N-n})(1-\alpha_{N-(n-1)})}\hat{j}_{(N-(n-1))0} \\ &+ \cdots + \sqrt{(1-\alpha_{N-n})\alpha_{N-(n-1)}\alpha_{N-(n-2)}\cdots\alpha_{N-3}(1-\alpha_{N-2})}\hat{j}_{(N-2)0} \\ &+ \sqrt{(1-\alpha_{N-n})\alpha_{N-(n-1)}\alpha_{N-(n-2)}\cdots\alpha_{N-2}(1-\alpha_{N-1})}\hat{j}_{(N-1)0} \\ &+ \sqrt{(1-\alpha_{N-n})\alpha_{N-(n-1)}\alpha_{N-(n-2)}\cdots\alpha_{N-2}(1-\alpha_{N-1})}\hat{j}_{(N-1)0} \\ &+ \sqrt{(1-\alpha_{N-n})\alpha_{N-(n-1)}\alpha_{N-(n-2)}\cdots\alpha_{N-1}}\hat{j}_{(N)0} + \underbrace{(\hat{u}_{(N-n)0} - \hat{v}^\dagger_{(N-n)0})}_{\text{noise}},\end{aligned}$$

$$\hat{o}^{(r)}_{(N-1)0} = -\sqrt{1-\alpha}\,\hat{j}_{10} - \sqrt{\alpha_1(1-\alpha_2)}\,\hat{j}_{20} - \sqrt{\alpha_1\alpha_2(1-\alpha_3)}\,\hat{j}_{30} - \cdots - \sqrt{\alpha_1\alpha_2\cdots\alpha_{N-2}(1-\alpha_{N-1})}\,\hat{j}_{(N-1)0} - \sqrt{\alpha_1\alpha_2\cdots\alpha_{N-2}\alpha_{N-1}}\,\hat{j}_{(N)0} + \underbrace{(\hat{b}_0 - \hat{a}_0^\dagger)}_{\text{entanglement}}. \tag{D17}$$

Here the discriminated mode is contained in $\hat{o}^{(r)}_{(N-1)0}$. For this choice of beam-splitter settings, this is a superposition of the $\hat{j}_{i0}$ temporal modes with equal phases between them, along with the entanglement resource. Meanwhile, the other N output modes contain orthogonal superposition modes with noise.

[1] H.-A. Bachor and T. C. Ralph, *A Guide to Experiments in Quantum Optics*, 3rd ed. (Wiley, New York, 2019).

[2] D. F. Walls and G. J. Milburn, *Quantum Optics* (Springer Science + Business Media, New York, 2007).

[3] P. P. Rohde, W. Mauerer, and C. Silberhorn, Spectral structure and decompositions of optical states, and their applications, New J. Phys. **9**, 91 (2007).

[4] V. Ansari, B. Brecht, J. Gil-Lopez, J. M. Donohue, J. Řeháček, Z. Hradil, L. L. Sánchez-Soto, and C. Silberhorn, Achieving the ultimate quantum timing resolution, PRX Quantum **2**, 010301 (2021).

[5] J. M. Donohue, V. Ansari, J. Řeháček, Z. Hradil, B. Stoklasa, M. Paúr, L. L. Sánchez-Soto, and C. Silberhorn, Quantum-Limited Time-Frequency Estimation through Mode-Selective Photon Measurement, Phys. Rev. Lett. **121**, 090501 (2018).

[6] W. Wasilewski, P. Kolenderski, and R. Frankowski, Spectral Density Matrix of a Single Photon Measured, Phys. Rev. Lett. **99**, 123601 (2007).

[7] E. Polino, M. Valeri, N. Spagnolo, and F. Sciarrino, Photonic quantum metrology, AVS Quantum Sci. **2**, 024703 (2020).

[8] J.-P. W. MacLean, S. Schwarz, and K. J. Resch, Reconstructing ultrafast energy-time-entangled two-photon pulses, Phys. Rev. A **100**, 033834 (2019).

[9] D. Su and T. C. Ralph, Quantum communication in the presence of a horizon, Phys. Rev. D **90**, 084022 (2014).

[10] S. Onoe, D. Su, and T. C. Ralph, Particle production and apparent decoherence due to an accelerated time delay, Phys. Rev. D **98**, 036011 (2018).

[11] S. Onoe and T. C. Ralph, Universal transformation of displacement operators and its application to homodyne tomography in differing relativistic reference frames, Phys. Rev. D **99**, 116001 (2019).

[12] J. Foo and T. C. Ralph, Continuous-variable quantum teleportation with vacuum-entangled Rindler modes, Phys. Rev. D **101**, 085006 (2020).

[13] J. Foo, S. Onoe, M. Zych, and T. C. Ralph, Generating multipartite entanglement from the quantum vacuum with a finite-lifetime mirror, New J. Phys. **22**, 083075 (2020).

[14] D. Su and T. C. Ralph, Decoherence of the Radiation from an Accelerated Quantum Source, Phys. Rev. X **9**, 011007 (2019).

[15] A. Eckstein, B. Brecht, and C. Silberhorn, A quantum pulse gate based on spectrally engineered sum frequency generation, Opt. Express **19**, 13770 (2011).

[16] V. Ansari, G. Harder, M. Allgaier, B. Brecht, and C. Silberhorn, Temporal-mode measurement tomography of a quantum pulse gate, Phys. Rev. A **96**, 063817 (2017).

[17] A. Christ, B. Brecht, W. Mauerer, and C. Silberhorn, Theory of quantum frequency conversion and type-II parametric down-conversion in the high-gain regime, New J. Phys. **15**, 053038 (2013).

[18] B. Brecht, A. Eckstein, A. Christ, H. Suche, and C. Silberhorn, From quantum pulse gate to quantum pulse shaper—engineered frequency conversion in nonlinear optical waveguides, New J. Phys. **13**, 065029 (2011).

[19] V. Ansari, J. M. Donohue, M. Allgaier, L. Sansoni, B. Brecht, J. Roslund, N. Treps, G. Harder, and C. Silberhorn, Tomography and Purification of the Temporal-Mode Structure of Quantum Light, Phys. Rev. Lett. **120**, 213601 (2018).

[20] K. F. Reim, J. Nunn, X.-M. Jin, P. S. Michelberger, T. F. M. Champion, D. G. England, K. C. Lee, W. S. Kolthammer, N. K. Langford, and I. A. Walmsley, Multipulse Addressing of a Raman Quantum Memory: Configurable Beam Splitting and Efficient Readout, Phys. Rev. Lett. **108**, 263602 (2012).

[21] D. V. Reddy and M. G. Raymer, Engineering temporal-mode-selective frequency conversion in nonlinear optical waveguides: From theory to experiment, Opt. Express **25**, 12952 (2017).

[22] F. Bussières, N. Sangouard, M. Afzelius, H. de Riedmatten, C. Simon, and W. Tittel, Prospective applications of optical quantum memories, J. Mod. Opt. **60**, 1519 (2013).

[23] X. Guo, Y. Mei, and S. Du, Single photon at a configurable quantum-memory-based beam splitter, Phys. Rev. A **97**, 063805 (2018).

[24] C. H. Bennett, G. Brassard, C. Crépeau, R. Jozsa, A. Peres, and W. K. Wootters, Teleporting an Unknown Quantum State via Dual Classical and Einstein-Podolsky-Rosen Channels, Phys. Rev. Lett. **70**, 1895 (1993).

[25] L. Vaidman, Teleportation of quantum states, Phys. Rev. A **49**, 1473 (1994).

[26] S. L. Braunstein and H. J. Kimble, Teleportation of Continuous Quantum Variables, Phys. Rev. Lett. **80**, 869 (1998).

[27] B. Brecht, D. V. Reddy, C. Silberhorn, and M. G. Raymer, Photon Temporal Modes: A Complete Framework for Quantum Information Science, Phys. Rev. X **5**, 041017 (2015).

[28] V. Ansari, J. M. Donohue, B. Brecht, and C. Silberhorn, Tailoring nonlinear processes for quantum optics with pulsed temporal-mode encodings, Optica **5**, 534 (2018).

[29] M. G. Raymer and I. A. Walmsley, Temporal modes in quantum optics: Then and now, Phys. Scr. **95**, 064002 (2020).

[30] N. Quesada and J. E. Sipe, Effects of time ordering in quantum nonlinear optics, Phys. Rev. A **90**, 063840 (2014).

[31] Y. Aharonov, D. Z. Albert, and L. Vaidman, Measurement process in relativistic quantum theory, Phys. Rev. D **34**, 1805 (1986).

[32] S. Popescu and L. Vaidman, Causality constraints on nonlocal quantum measurements, Phys. Rev. A **49**, 4331 (1994).

[33] R. D. Sorkin, in *Directions in General Relativity: Proceedings of the International Symposium in Honor of the 60th Birthdays of Dieter Brill and Charles Misner*, edited by B.-L. Hu and T. A. Jacobsen (Cambridge University Press, Cambridge, 1993), Vol. 2, pp. 293–305.

[34] D. Beckman, D. Gottesman, A. Kitaev, and J. Preskill, Measurability of Wilson loop operators, Phys. Rev. D **65**, 065022 (2002).

[35] S.-Y. Lin, Notes on nonlocal projective measurements in relativistic systems, Ann. Phys. (NY) **351**, 773 (2014).

[36] C. J. Fewster and R. Verch, Quantum fields and local measurements, Commun. Math. Phys. **378**, 851 (2020).

[37] J. de Ramón, M. Papageorgiou, and E. Martín-Martínez, Relativistic causality in particle detector models: Faster-than-light signaling and impossible measurements, Phys. Rev. D **103**, 085002 (2021).

[38] E. Martín-Martínez, T. R. Perche, and B. d. S. L. Torres, Broken covariance of particle detector models in relativistic quantum information, Phys. Rev. D **103**, 025007 (2021).

[39] O. Oreshkov, F. Costa, and C. Brukner, Quantum correlations with no causal order, Nat. Commun. **3**, 1092 (2012).

[40] E. Schmidt, in *Integralgleichungen und Gleichungen mit Unendlich Vielen Unbekannten*, edited by A. Pietsch (Vieweg+Teubner, Wiesbaden, 1989), pp. 190–233.

[41] A. Ekert and P. L. Knight, Entangled quantum systems and the schmidt decomposition, Am. J. Phys. **63**, 415 (1995).

[42] A. Acín, A. Andrianov, L. Costa, E. Jané, J. I. Latorre, and R. Tarrach, Generalized Schmidt Decomposition and Classification of Three-Quantum-Bit States, Phys. Rev. Lett. **85**, 1560 (2000).

[43] H. A. Carteret, A. Higuchi, and A. Sudbery, Multipartite generalization of the Schmidt decomposition, J. Math. Phys. **41**, 7932 (2000).

[44] S. Pirandola and S. Mancini, Quantum teleportation with continuous variables: A survey, Laser Phys. **16**, 1418 (2006).

[45] T. C. Ralph, Interferometric tests of teleportation, Phys. Rev. A **65**, 012319 (2001).

[46] J. G. Webb, T. C. Ralph, and E. H. Huntington, Homodyne measurement of the average photon number, Phys. Rev. A **73**, 033808 (2006).

[47] M. Cooper, L. J. Wright, C. Söller, and B. J. Smith, Experimental generation of multi-photon Fock states, Opt. Express **21**, 5309 (2013).

[48] M. Harris, G. N. Pearson, C. A. Hill, and J. M. Vaughan, Higher moments of scattered light fields by heterodyne analysis, Appl. Opt. **33**, 7226 (1994).

[49] T. C. Ralph, P. K. Lam, and R. E. S. Polkinghorne, Characterizing teleportation in optics, J. Opt. B **1**, 483 (1999).

[50] T. C. Ralph, All-optical quantum teleportation, Opt. Lett. **24**, 348 (1999).

[51] S. Liu, Y. Lou, and J. Jing, Orbital angular momentum multiplexed deterministic all-optical quantum teleportation, Nat. Commun. **11**, 3875 (2020).

[52] U. M. Titulaer and R. J. Glauber, Density operators for coherent fields, Phys. Rev. **145**, 1041 (1966).

[53] C. Branciard, M. Araújo, A. Feix, F. Costa, and Č. Brukner, The simplest causal inequalities and their violation, New J. Phys. **18**, 013008 (2015).

[54] A. A. Abbott, C. Giarmatzi, F. Costa, and C. Branciard, Multipartite causal correlations: Polytopes and inequalities, Phys. Rev. A **94**, 032131 (2016).

[55] K. F. Reim, P. Michelberger, K. C. Lee, J. Nunn, N. K. Langford, and I. A. Walmsley, Single-Photon-Level Quantum Memory at Room Temperature, Phys. Rev. Lett. **107**, 053603 (2011).

[56] D. V. Reddy and M. G. Raymer, High-selectivity quantum pulse gating of photonic temporal modes using all-optical Ramsey interferometry, Optica **5**, 423 (2018).

[57] B. Brecht, A. Eckstein, R. Ricken, V. Quiring, H. Suche, L. Sansoni, and C. Silberhorn, Demonstration of coherent time-frequency Schmidt mode selection using dispersion-engineered frequency conversion, Phys. Rev. A **90**, 030302(R) (2014).

[58] R. B. Mann and T. C. Ralph, Relativistic quantum information, Classical Quantum Grav. **29**, 220301 (2012).

[59] H. Vahlbruch, M. Mehmet, K. Danzmann, and R. Schnabel, Detection of 15 db Squeezed States of Light and their Application for the Absolute Calibration of Photoelectric Quantum Efficiency, Phys. Rev. Lett. **117**, 110801 (2016).